

Response of an in-core neutron detector to a
vibrating absorber based on the detector
adjoint function

by

Mohammad Salih Abdul Rahman Salih

A Thesis Submitted to the
Graduate Faculty in Partial Fulfillment of the
Requirements for the Degree of
MASTER OF SCIENCE

Major: Nuclear Engineering

Signatures have been redacted for privacy

Iowa State University
Ames, Iowa

1980

TABLE OF CONTENTS

	Page
I. INTRODUCTION	1
II. LITERATURE SURVEY	3
III. THEORETICAL DEVELOPMENT OF THE DETECTOR RESPONSE TO A MOVING ABSORBER	7
A. Multigroup Perturbation Theory and the Adjoint Function	7
B. The Time-Dependent Neutron Diffusion Equation and the Detector Adjoint Function	10
C. Response to a Moving Absorber	20
D. Extension to a Multigroup Formulation	22
IV. INPUT DATA PREPARATION FOR WHIRLAWAY AND LEOPARD COMPUTER CODES	28
A. UTR-10 Model Used in this Work	28
B. Description of the Input Data for LEOPARD	34
C. LEOPARD Output Which is Used As Input Data to the WHIRLAWAY Code	40
D. WHIRLAWAY Input Data	42
E. WHIRLAWAY Output Description	50
V. PROCEDURES AND RESULTS	52
A. K_{eff} Search	52
B. The Adjoint Flux Calculation for Different Detector Positions	65
C. Detector Response Function	71
VI. CONCLUSIONS	75
VII. SUGGESTIONS FOR FUTURE WORK	77

	Page
VIII. BIBLIOGRAPHY	78
IX. ACKNOWLEDGMENTS	80
X. APPENDIX A: COMPUTER PROGRAMS FOR PLOTTING	81
A. The One-Dimensional Plot Computer Program	81
B. Using Tapes in Running WHIRLAWAY Code and the Two-Dimensional Plot Computer Program	82
XI. APPENDIX B	87
A. Description of Vibrator Assembly	87
B. Preliminary Safety Analysis Report for the Proposed Experiment	91
XII. APPENDIX C: THE REQUIRED JCL FOR RUNNING WHIRLAWAY CODE	95

I. INTRODUCTION

In recent years, the response of a neutron detector to a reactor component vibration has been one of the areas of interest in reactor noise analysis. Using theoretical investigations of noise analysis, the neutron noise diagnostics for a two-dimensional control rod vibration in a pressurized water reactor (PWR) has been developed by Pazsit and Analytis (14). Also, by using the adjoint technique, Pazsit (13) has developed a one-dimensional semi-analytical method for two-group theory of noise in reflected reactors. The detector response to parametric fluctuations in a boiling water reactor (BWR) has been investigated by Dam (3).

Analytis (1), attempted to develop the concept of local and global components of neutron noise in bare homogeneous water moderated reactors in three dimensions.

The aim of the present work can be summarized as follows:

1. To determine analytically the detector response to a vibrating absorber located in the core by using a three-dimensional calculation for the adjoint function.
2. To develop a preliminary design for a vibrator that could be used in the UTR-10 reactor for a noise source.

In this work, a three-dimensional model of the UTR-10

reactor has been developed where for calculational accuracy, each assembly in the core has been treated individually. A three-dimensional computer code WHIRLAWAY has been used to calculate the regular flux and the detector adjoint function, both of which are required in the theoretical analysis of the reactor. The nuclear parameters, which are used as input data for WHIRLAWAY, have been calculated by using the LEOPARD code. A preliminary safety analysis report for the proposed experiment has also been carried out.

II. LITERATURE SURVEY

Over the past few years, studies in noise analysis have been reviewed by Analytis (1), Dam (3, 4), Greenspan (7, 8), Kosaly (11, 12), and Pazzit (13, 14). Analytis (1) shows that under certain limitations, the two-group treatment of the neutron noise and the subsequent derivation of the two components, is equivalent to the one-group theory in which the slowing down of the fast neutrons is taken into account through an appropriately chosen slowing down kernel. For purpose of investigation, he applied the theory that he developed to the local component of the neutron noise induced by a vibrating thin absorber in a two-dimensional cylindrical reactor and the neutron noise related to moderator density variation, in a multi-channel model of a three-dimensional slab reactor.

Dam (3) used two-group theory for his development of the neutron detector response to a nuclear parametric fluctuation. Also, he defined an equation for the adjoint function which depends on the detector cross-section Σ_d . Then, he applied the theory that he developed to calculate the two-group detector adjoint functions for a reactor core having a composition typical of a boiling water reactor. In his later paper (4), he extended his theoretical development to the adjoint transport theory in the frequency domain to

define the detector and system dependent transfer function. Also, he explained the application of the adjoint theory in the frequency domain.

Greenspan (7) generalized the total importance balance condition for time-dependent problems. Also, he stated that this condition provides a unified formulation that is useful for deducing: 1) the equations, boundary conditions, and time conditions satisfied by adjoint functions of different physical meaning, and 2) the mathematical foundation for different applications of adjoint functions. Specific contributions were included in his work: 1) the generalization of the adjoint equation to include a precursor adjoint source term, 2) the definition of the importance function for a precursors detector, and 3) the generalization of the adjoint space formulation for accumulated detector response. Then, he attempted some applications of the adjoint function (8).

Kosaly and Mesko (12) stated that the noise-field in a large BWR core is strongly space dependent, moreover, there is a component in the noise which acts in a local manner, that is, its behavior is influenced mainly by the disturbances which are close to the detector. Then, he developed a one-group diffusion theory model to calculate the response of the neutron field to a propagating disturbance of moderator density fluctuation. He defined the neutron noise in a BWR as the sum of a local contribution driven by the bubbles in the

vicinity of the detector, plus a global background driven by fluctuations of reactivity. He turned to a two-group theory to identify one term in the solution with the local component of the noise field. More recently Kosaly has published some remarks on a few problems in the theory of power reactor noise (11).

Pazsit (13) used a one-dimensional semi-analytic calculation to describe the response of a neutron detector to a moving absorber for the two-group diffusion model based on the adjoint technique. He carried through the calculation of the static fluxes and the static adjoints. Then, he developed the solution of the time-dependent problem and the calculation of the detector adjoint functions. Extension of the one-dimensional diagnostic model to two spatial dimensions in a bare homogeneous PWR core has been done by Pazsit and Analytis (14). The two-dimensional Green's function for a bare rectangular core was derived. It was found to have a more rapid spatial variation in two dimensions which means more pronounced space dependent effects in contrast to the one-dimensional case.

Huang (10) used the adjoint space models for predicting the response of a neutron detector to core parametric fluctuations. The purpose of his work was to develop a

generalized model using the detector adjoint function for the detector response to random fluctuation of reactor core parameters and to support his model by physical interpretation as well as experimental verification. He stated in his conclusion that the detector model he developed is more realistic and sophisticated than those developed by other investigators (3, 11, 12, 13) due to the facts: 1) both the location and the size of the detector as well as the noise source were taken into account, 2) the modeling calculations, using the WHIRLAWAY-H code, were based on a three-dimensional model of a UTR-10 type reactor and were verified by experimental measurements. A multigroup formulation was used and the adjoint fluxes can be taken as complex quantities if it is required.

III. THEORETICAL DEVELOPMENT OF THE DETECTOR RESPONSE TO A MOVING ABSORBER

In this chapter, the response of a reactor to a moving absorber is developed using the detector adjoint function. As background for this, the properties of the regular adjoint function as used in perturbation theory are reviewed. The detector adjoint formulation is then developed using one-group theory as an example and the extension to a multigroup analysis is then considered.

A. Multigroup Perturbation Theory and the Adjoint Function

Consider multigroup perturbation theory and the multigroup diffusion equation:

$$\underline{M}\phi = \frac{1}{K} \underline{F}\phi \quad (3.1)$$

where

\underline{M} is the diffusion matrix

\underline{F} is the fission matrix.

Due to any noise source in the reactor resulting from a change in a reactor parameter, the reactivity will change. To calculate the reactivity change, use is made of the inner product between two G-dimensional vectors $\underline{f}(\underline{r})$ and $\underline{g}(\underline{r})$

$$(f, g) = \int_V d\underline{r}^3 [f_1^*(\underline{r})g_1(\underline{r}) + f_2^*(\underline{r})g_2(\underline{r}) + \dots] \quad (3.2)$$

where $f^*(\underline{r})$ is the complex conjugate of $f(\underline{r})$. From this the adjoint of the operator \underline{M} and \underline{F} can be defined as

$$(\underline{M}^\dagger \underline{f}, \underline{g}) = (\underline{f}, \underline{Mg})$$

or

$$(\underline{F}^\dagger \underline{f}, \underline{g}) = (\underline{f}, \underline{Fg}) \quad (3.3)$$

where M^\dagger and F^\dagger are the adjoint operators. It should be recalled that the multigroup problem is not self-adjoint.

The equation adjoint to Equation (3.1) is

$$M^\dagger \phi^\dagger = \frac{1}{K} F^\dagger \phi^\dagger. \quad (3.4)$$

For the reactor equation it can be shown that $M^\dagger = M^T$ and $F^\dagger = F^T$ where T indicates that the transpose of the original matrix is to be taken.

Due to the core perturbation, the matrix operators will change as follows

$$\underline{M}' = \underline{M} + \delta \underline{M}$$

and

$$\underline{F}' = \underline{F} + \delta \underline{F}. \quad (3.5)$$

It can be shown that the corresponding reactivity change is

$$\Delta \rho = \frac{[\phi^\dagger, [\delta \underline{F} - \delta \underline{M}] \phi]}{(\phi^\dagger, \underline{F} \phi)}. \quad (3.6)$$

As an example of the use of Equation (3.6), consider the two-group problem where it is assumed that all fission neutrons are released in group one

$$-\nabla \cdot D_1 \nabla \phi_1 + \Sigma_{R_1} \phi_1 = \frac{1}{K} (\nu_1 \Sigma_{f_1} \phi_1 + \nu_2 \Sigma_{f_2} \phi_2) \quad (3.7)$$

$$-\Sigma_{s_{12}} \phi_1 - \nabla \cdot D_2 \nabla \phi_2 + \Sigma_{a_2} \phi_2 = 0. \quad (3.8)$$

Put Equations (3.7) and (3.8) in a matrix form

$$\begin{bmatrix} -\nabla \cdot D_1 \nabla + \Sigma_{R_1} & 0 \\ -\Sigma_{s_{12}} & -\nabla \cdot D_2 \nabla + \Sigma_{a_2} \end{bmatrix} \begin{bmatrix} \phi_1 \\ \phi_2 \end{bmatrix} = \frac{1}{K} \begin{bmatrix} \nu_1 \Sigma_{f_1} & \nu_2 \Sigma_{f_2} \\ 0 & 0 \end{bmatrix} \begin{bmatrix} \phi_1 \\ \phi_2 \end{bmatrix} \quad (3.9)$$

$\underline{\underline{M}} \quad \underline{\phi} \quad \underline{\underline{F}} \quad \underline{\phi}$

and the adjoint equation for Equation (3.9) is

$$\begin{bmatrix} -\nabla \cdot D_1 \nabla + \Sigma_{R_1} & -\Sigma_{s_{12}} \\ 0 & -\nabla \cdot D_2 \nabla + \Sigma_{a_2} \end{bmatrix} \begin{bmatrix} \phi_1^\dagger \\ \phi_2^\dagger \end{bmatrix} = \frac{1}{K} \begin{bmatrix} \nu_1 \Sigma_{f_1} & 0 \\ \nu_2 \Sigma_{f_2} & 0 \end{bmatrix} \begin{bmatrix} \phi_1^\dagger \\ \phi_2^\dagger \end{bmatrix}. \quad (3.10)$$

Suppose there is no change in the fission cross section, i.e., $\delta F = 0$, and the change in the thermal absorption cross section is represented by $\delta \Sigma_{a_2}$, then

$$\delta \underline{\underline{M}} = \begin{bmatrix} 0 & 0 \\ 0 & \delta \Sigma_{a_2} \end{bmatrix}. \quad (3.11)$$

The corresponding reactivity change is then

$$\Delta\rho = \frac{\int_{\mathbf{v}} d\mathbf{r}^3 (\phi_1^\dagger \phi_2^\dagger) \begin{pmatrix} 0 & 0 \\ 0 & \delta\Sigma_{a_2} \end{pmatrix} \begin{pmatrix} \phi_1 \\ \phi_2 \end{pmatrix}}{\int_{\mathbf{v}} d\mathbf{r}^3 (\phi_1^\dagger \phi_2^\dagger) \begin{pmatrix} \nu_1 \Sigma_{f_1} & \nu_2 \Sigma_{f_2} \\ 0 & 0 \end{pmatrix} \begin{pmatrix} \phi_1 \\ \phi_2 \end{pmatrix}} . \quad (3.12)$$

Set the weighted total neutron production rate term in the denominator of Equation (3.12) equal to a constant, say c , and simplify the equation to obtain

$$\Delta\rho = -\frac{1}{c} \int_{\mathbf{v}} d^3r \phi_2^\dagger \delta\Sigma_{a_2} \phi_2 . \quad (3.13)$$

The term $\delta\Sigma_{a_2} \phi_2$ represents the rate of neutron removal due to the absorber cross section change and the regular adjoint flux ϕ_2^\dagger represents the "importance" to the chain reaction of the neutrons that have been absorbed. In this sense, ϕ^\dagger is sometimes called the neutron importance function.

B. The Time-Dependent Neutron Diffusion Equation and the Detector Adjoint Function

In this section, the one-group time dependent neutron diffusion equations are used to derive the concept of the detector adjoint function (3).

The one-group time dependent diffusion equations are

$$\nabla \cdot D \nabla \phi + \nu \Sigma_f (1-\beta) \phi - \Sigma_a \phi + \Sigma \lambda_i C_i = \frac{1}{V} \frac{\partial \phi}{\partial t} \quad (3.14)$$

$$\beta \nu \Sigma_f \phi - \lambda_i C_i = \frac{\partial C_i}{\partial t} . \quad (3.15)$$

For fluctuations in the nuclear parameters D and Σ_a

$$D = D_0 + \delta D \quad (3.16)$$

$$\Sigma_a = \Sigma_{a_0} + \delta \Sigma_a.$$

These fluctuations will cause fluctuations in the flux and the concentration of the delayed neutron precursors as follows

$$\phi = \phi_0 + \delta \phi \quad (3.17)$$

$$C_i = C_{i_0} + \delta C_i$$

where D_0 , Σ_{a_0} , ϕ_0 and C_{i_0} are the steady state values.

Substituting Equation (3.16) and (3.17) into Equation (3.14) and (3.15) yields

$$\begin{aligned} & \nabla \cdot (D_0 + \delta D) \nabla (\phi_0 + \delta \phi) + v \Sigma_f (1 - \beta) (\phi_0 + \delta \phi) \\ & - (\Sigma_{a_0} + \delta \Sigma_a) (\phi_0 + \delta \phi) + \Sigma \lambda_i (C_{i_0} + \delta C_i) \\ & = \frac{1}{\bar{V}} \frac{\partial (\phi_0 + \delta \phi)}{\partial t} \end{aligned} \quad (3.18)$$

and

$$\beta v \Sigma_f (\phi_0 + \delta \phi) - \lambda_i (C_{i_0} + \delta C_i) = \frac{\partial (C_{i_0} + \delta C_i)}{\partial t}. \quad (3.19)$$

Subtracting the steady state terms and neglecting the second order terms yields

$$\begin{aligned} \nabla \cdot D_0 \nabla \delta\phi + v \Sigma_f (1-\beta) \delta\phi - \Sigma_{a_0} \delta\phi + \Sigma \lambda_i \delta C_i \\ = \frac{1}{V} \frac{\partial \phi}{\partial t} + \delta \Sigma_a \phi_0 - \nabla \cdot \delta D \nabla \phi_0 \end{aligned} \quad (3.20)$$

and

$$\beta v \Sigma_f \delta\phi - \lambda_i \delta C_i = \frac{\partial \delta C_i}{\partial t} . \quad (3.21)$$

Taking the Laplace transform of Equations (3.20) and (3.21) yields

$$\begin{aligned} \nabla \cdot D_0 \nabla \Delta\phi + v \Sigma_f (1-\beta) \Delta\phi - \Sigma_{a_0} \Delta\phi + \Sigma \lambda_i \Delta C_i \\ = \frac{S}{V} \Delta\phi + \Delta \Sigma_a \phi_0 - \nabla \cdot \Delta D \nabla \phi_0 \end{aligned} \quad (3.22)$$

and

$$\beta v \Sigma_f \Delta\phi - \lambda_i \Delta C_i = S \Delta C_i . \quad (3.23)$$

Solve Equation (3.23) for ΔC_i to find

$$\Delta C_i = \frac{\beta v \Sigma_f \Delta\phi}{\lambda_i + S} . \quad (3.24)$$

Substitute Equation (3.24) into Equation (3.22) to obtain the equation which describes the spatial and frequency dependent flux

$$\begin{aligned} \nabla \cdot D_0 \nabla \Delta\phi + v \Sigma_f (1-\beta) \Delta\phi - \Sigma_{a_0} \Delta\phi + \Sigma \lambda_i \frac{\beta v \Sigma_f \Delta\phi}{\lambda_i + S} \\ = \frac{S}{V} \Delta\phi + \Delta \Sigma_a \phi_0 - \nabla \cdot \Delta D \nabla \phi_0 , \end{aligned} \quad (3.25)$$

where the noise source Q is identified as

$$Q = \Delta \Sigma_a \phi_0 - \nabla \cdot \Delta D \nabla \phi_0 . \quad (3.26)$$

Define an equation for an adjoint function ϕ^\dagger dependent on the detector cross section Σ_d

$$\begin{aligned} \nabla \cdot D_0 \nabla \phi^\dagger + v \Sigma_f (1-\beta) \phi^\dagger - \Sigma_{a_0} \phi^\dagger + v \Sigma_f \phi^\dagger \Sigma \frac{\beta_i \lambda_i}{S + \lambda_i} \\ = -\Sigma_d + \frac{S}{V} \phi^\dagger. \end{aligned} \quad (3.27)$$

In this case, ϕ^\dagger is a complex quantity

$$\phi^\dagger = \psi_R + j\chi_I.$$

Now, multiply Equation (3.25) by ϕ^\dagger and Equation (3.27) by $\Delta\phi$ to obtain

$$\begin{aligned} \phi^\dagger \nabla \cdot D_0 \nabla \Delta\phi + \phi^\dagger v \Sigma_f (1-\beta) \Delta\phi - \phi^\dagger \Sigma_{a_0} \Delta\phi + \phi^\dagger v \Sigma_f \Delta\phi \\ \times \Sigma \frac{\lambda_i \beta_i}{S + \lambda_i} = \phi^\dagger \frac{S}{V} \Delta\phi + \phi^\dagger \Delta \Sigma_{a_0} \phi_0 - \phi^\dagger \nabla \cdot \Delta D \nabla \phi \end{aligned} \quad (3.28)$$

and

$$\begin{aligned} \Delta\phi \nabla \cdot D_0 \nabla \phi^\dagger + \Delta\phi v \Sigma_f (1-\beta) \phi^\dagger - \Delta\phi \Sigma_{a_0} \phi^\dagger + \Delta\phi v \Sigma_f \phi^\dagger \\ \times \Sigma \frac{\lambda_i \beta_i}{S + \lambda_i} = -\Delta\phi \Sigma_d + \Delta\phi \frac{S}{V} \phi^\dagger. \end{aligned} \quad (3.29)$$

Subtract Equation (3.29) from Equation (3.28)

$$\begin{aligned} \phi^\dagger \nabla \cdot D_0 \nabla \Delta\phi - \Delta\phi \nabla \cdot D_0 \nabla \phi^\dagger = \phi^\dagger \Delta \Sigma_{a_0} \phi_0 - \phi^\dagger \nabla \cdot \Delta D \nabla \phi_0 \\ + \Delta\phi \Sigma_d. \end{aligned} \quad (3.30)$$

Integrate Equation (3.30) over the reactor volume

$$\begin{aligned}
& \int_V [\phi^\dagger \nabla \cdot D_0 \nabla \Delta \phi - \Delta \phi \nabla \cdot D_0 \nabla \phi^\dagger] dV \\
&= \int_V [\phi^\dagger \Delta \Sigma_a \phi_0 - \phi^\dagger \nabla \cdot \Delta D \nabla \phi_0] dV + \int_V \Sigma_d \Delta \phi dV. \quad (3.31)
\end{aligned}$$

In Equation (3.31) the term $\phi^\dagger \nabla \cdot \Delta D \nabla \phi_0$ may be written as

$$\nabla \cdot \phi^\dagger \Delta D \nabla \phi - \nabla \phi^\dagger \cdot \Delta D \nabla \phi. \quad (3.32)$$

By taking the integration over the reactor volume it follows that

$$\int_V \phi^\dagger \nabla \cdot \Delta D \nabla \phi_0 dV = \int_V \nabla \cdot \phi^\dagger \Delta D \nabla \phi_0 dV - \int_V \nabla \phi^\dagger \cdot \Delta D \nabla \phi_0 dV. \quad (3.33)$$

The first term on the RHS of Equation (3.33) is equal to zero by applying Green's divergence theorem. Equation (3.31) becomes then
$$\int_V \Sigma_d \Delta \phi dV = - \int_V [\Delta \Sigma_a \phi_0 \phi^\dagger + \Delta D \nabla \phi^\dagger \cdot \nabla \phi_0] dV. \quad (3.34)$$

The LHS of Equation (3.34) represents the response of the detector having cross section Σ_d to the fluctuating flux $\Delta \phi$.

The detector adjoint function ϕ^\dagger which appears on the RHS of Equation (3.34) can be regarded as describing the "field of view" of the neutron detector (3).

Equation (3.27) which upon rearrangement is

$$\nabla \cdot D_0 \nabla \phi^\dagger + \nu \Sigma_f \phi^\dagger \left\{ 1 - \frac{\beta_i S}{S + \lambda_i} \right\} - \frac{S}{V} \phi^\dagger - \Sigma_{a_0} \phi^\dagger = -\Sigma_d \quad (3.35)$$

may be expressed in terms of the zero power reactor transfer function.

To obtain the reactivity transfer function start with the reactor kinetic equations

$$\frac{dn}{dt} = \frac{\rho - \beta}{\ell} n + \sum \lambda_i C_i \quad (3.36)$$

$$\frac{dC_i}{dt} = \frac{\beta_i}{\ell} n - \lambda_i C_i. \quad (3.37)$$

Which upon using the small signal model become

$$\frac{d\delta n}{dt} = \frac{\rho n_0}{\ell} - \frac{\beta}{\ell} \delta n + \sum \lambda_i C_i \quad (3.38)$$

$$\frac{d\delta C_i}{dt} = \frac{\beta_i}{\ell} \delta n - \lambda_i \delta C_i. \quad (3.39)$$

Taking the Laplace transform of Equations (3.38) and (3.39) yields

$$SN = \frac{\rho(S)n_0}{\ell} - \frac{\beta}{\ell} N + \sum \lambda_i C_i \quad (3.40)$$

$$SC_i = \frac{\beta_i}{\ell} N - \lambda_i C_i. \quad (3.41)$$

Solve Equation (3.41) for C_i ,

$$C_i = \frac{(\beta_i/\ell)N}{S + \lambda_i}$$

and substitute into Equation (3.40) to obtain

$$SN = \frac{\rho(S)n_0}{\ell} - \frac{\beta}{\ell} N + \sum \lambda_i \frac{(\beta_i/\ell)N}{S+\lambda_i}$$

or

$$SN = \frac{\rho(S)n_0}{\ell} - \frac{N}{\ell} \sum \beta_i + \frac{N}{\ell} \sum \frac{\lambda_i \beta_i}{S+\lambda_i}$$

$$SN = \frac{\rho(S)n_0}{\ell} - \frac{N}{\ell} \sum \frac{\beta_i S}{S+\lambda_i}$$

$$\frac{N}{\rho} = \frac{n_0}{\ell S + \sum \frac{\beta_i S}{S+\lambda_i}} \quad (3.42)$$

Returning to Equation (3.35) multiply and divide the term $-\frac{S}{V}\phi^\dagger$ by $v\Sigma_f$

$$-\frac{S}{V} \frac{v\Sigma_f}{v\Sigma_f} \phi^\dagger$$

and note that

$$\ell = \frac{\ell_0}{K_{\text{eff}}} = \frac{1}{v\Sigma_a} \frac{\Sigma_a}{v\Sigma_f} = \frac{1}{v\Sigma_f}$$

So that

$$-\frac{S}{V} \frac{v\Sigma_f}{v\Sigma_f} \phi^\dagger = -S\ell v\Sigma_f \phi^\dagger \quad (3.43)$$

Thus, in Equation (3.35) the two terms

$-\nu\Sigma_f\phi^\dagger \sum \frac{\beta_i S}{S+\lambda_i} - \frac{S}{V}\phi^\dagger$ can be rearranged and written as follows:

$$-v \Sigma_f \phi^\dagger \left(\Sigma \frac{\beta_i S}{S + \lambda_i} + \ell S \right)$$

$$\text{where } H(S) = \frac{N/n_0}{\rho(S)} = \frac{1}{\ell S + \Sigma \frac{\beta_i S}{S + \lambda_i}} .$$

Equation (3.35) becomes then

$$\nabla \cdot D_0 \nabla \phi^\dagger + v \Sigma_f \phi^\dagger \left\{ 1 - \frac{1}{H(S)} \right\} - \Sigma_a \phi^\dagger = -\Sigma_d . \quad (3.44)$$

Note that due to the presence of the detector cross section term, Equation (3.44) is a nonhomogeneous equation and may be solved using the method of Green's function (9).

As noted before, ϕ^\dagger is a complex quantity, and $S = j\omega$, so after introducing these into Equation (3.35) it follows that

$$\begin{aligned} \nabla \cdot D_0 \nabla (\psi + j\chi) + v \Sigma_f (\psi + j\chi) \left\{ 1 - \Sigma \frac{\beta_i j\omega}{j\omega + \lambda_i} \right\} \\ - \frac{j\omega}{V} (\psi + j\chi) - \Sigma_a (\psi + j\chi) = -\Sigma_d \end{aligned}$$

or

$$\begin{aligned} \nabla \cdot D_0 \nabla \psi + j \nabla \cdot D_0 \nabla \chi + v \Sigma_f (\psi + j\chi) \left\{ 1 - \Sigma \frac{\beta_i j\omega (-j\omega + \lambda_i)}{\omega^2 + \lambda_i^2} \right\} \\ - \frac{j\omega}{V} \psi + \frac{\omega}{V} \chi - \Sigma_a \psi - j \Sigma_a \chi = -\Sigma_d . \end{aligned} \quad (3.45)$$

Expanding the { } in the third term of Equation (3.45)

$$\begin{aligned}
& \left\{ 1 - \Sigma \frac{\beta_i j \omega (-j \omega + \lambda_i)}{\omega^2 + \lambda_i^2} \right\} \\
&= 1 - \Sigma \frac{\beta_i \omega^2 + \beta_i j \omega \lambda_i}{\omega^2 + \lambda_i^2} \\
&= 1 - \Sigma \frac{\beta_i \omega^2}{\omega^2 + \lambda_i^2} - j \Sigma \frac{\beta_i \omega \lambda_i}{\omega^2 + \lambda_i^2}
\end{aligned}$$

and expanding the third term further yields

$$\begin{aligned}
& \nu \Sigma_f \psi \left(1 - \Sigma \frac{\beta_i \omega^2}{\omega^2 + \lambda_i^2} - j \Sigma \frac{\beta_i \omega \lambda_i}{\omega^2 + \lambda_i^2} \right) + \nu \Sigma_f j \chi \left(1 - \Sigma \frac{\beta_i \omega^2}{\omega^2 + \lambda_i^2} \right. \\
& \quad \left. - j \Sigma \frac{\beta_i \omega \lambda_i}{\omega^2 + \lambda_i^2} \right).
\end{aligned}$$

For one group of delayed neutrons this becomes

$$\begin{aligned}
& \nu \Sigma_f \psi \left(1 - \frac{\beta \omega^2}{\omega^2 + \lambda^2} - j \frac{\beta \omega \lambda}{\omega^2 + \lambda^2} \right) + \nu \Sigma_f j \chi \left(1 - \frac{\beta \omega^2}{\omega^2 + \lambda^2} \right. \\
& \quad \left. - j \frac{\beta \omega \lambda}{\omega^2 + \lambda^2} \right).
\end{aligned}$$

Then, the complete equation is

$$\begin{aligned}
& \nabla \cdot D_0 \nabla \psi + j \nabla \cdot D_0 \nabla \chi + \nu \Sigma_f \psi \left(1 - \frac{\beta \omega^2}{\omega^2 + \lambda^2} - j \frac{\beta \omega \lambda}{\omega^2 + \lambda^2} \right) \\
& + \nu \Sigma_f j \chi \left(1 - \frac{\beta \omega^2}{\omega^2 + \lambda^2} - j \frac{\beta \omega \lambda}{\omega^2 + \lambda^2} \right) - j \frac{\omega}{V} \psi + \frac{\omega}{V} \chi \\
& - \Sigma_{a_0} \psi - j \Sigma_{a_0} \chi = -\Sigma_d.
\end{aligned} \tag{3.46}$$

From Equation (3.46) the real and the imaginary parts can be separated as follows:

Real part:

$$\begin{aligned} \nabla \cdot D_0 \nabla \psi + v \Sigma_f \psi \left(1 - \frac{\beta \omega^2}{\omega^2 + \lambda^2}\right) + v \Sigma_f \chi \frac{\beta \omega \lambda}{\omega^2 + \lambda^2} \\ + \frac{\omega}{V} \chi - \Sigma_{a_0} \psi = -\Sigma_d \end{aligned} \quad (3.47)$$

Imaginary part:

$$\begin{aligned} \nabla \cdot D_0 \nabla \chi - v \Sigma_f \psi \frac{\beta \omega \lambda}{\omega^2 + \lambda^2} + v \Sigma_f \chi \left(1 - \frac{\beta \omega^2}{\omega^2 + \lambda^2}\right) \\ - \frac{\omega}{V} \psi - \Sigma_{a_0} \chi = 0. \end{aligned} \quad (3.48)$$

Therefore, it follows that to obtain the detector adjoint function, a coupled set of neutron diffusion like equations must be solved where the size of the system of equations is two times the number of energy groups used in the analysis. The resulting equations are of the form normally solved with neutron diffusion computer codes. Note that the code must be capable of treating an external source and upscattering. Equations (3.47) and (3.48) may be simplified by noting that in the plateau region of the transfer function, χ is very much smaller than ψ so that effectively, only Equation (3.47) need be solved in the form

$$\nabla \cdot D \nabla \psi + v \Sigma_f \psi \left(1 - \frac{\beta \omega^2}{\omega^2 + \lambda^2}\right) - \Sigma_{a_0} \psi = -\Sigma_d. \quad (3.47a)$$

C. Response to a Moving Absorber

Neglect the term $\Delta D \nabla \phi^\dagger \cdot \nabla \phi_0$ in Equation (3.34), to obtain

$$\int_V \Sigma_d \Delta \phi dV = - \int_V \Delta \Sigma_a \phi_0 \phi^\dagger dV \quad (3.49)$$

This could be written as

$$\int_V \Sigma_d(\mathbf{x}) \Delta \phi(\mathbf{x}, \omega) d\mathbf{x} = \int_V Q(\mathbf{x}, \omega) \phi^\dagger(\mathbf{x}, \omega) d\mathbf{x} \quad (3.50)$$

Where Σ_d is the detector cross section which can be represented by

$$\Sigma_d = \delta(\mathbf{x} - \mathbf{x}_0). \quad (3.51)$$

Then the LHS of Equation (3.50) becomes

$$\int_V \delta(\mathbf{x} - \mathbf{x}_0) \Delta \phi = \Delta \phi(\mathbf{x}_0)$$

and Q in the RHS of Equation (3.50) can be represented by

$$Q = \Delta \Sigma_a \phi_0. \quad (3.52)$$

Then the RHS of Equation (3.50) becomes

$$\int_V \Delta \Sigma_a \phi_0 \phi^\dagger d\mathbf{x}.$$

Then the complete equation is

$$\Delta\phi = \int_V \Delta\Sigma_a \phi_0 \phi^\dagger dx, \quad (3.53)$$

where ϕ_0 in Equation (3.53) represents the steady state flux.

Now, consider that

$$\Delta\Sigma_a = \gamma \int_{-\infty}^{\infty} [\delta(x-x_p - \epsilon(t)) - \delta(x-x_p)] e^{i\omega t} dt. \quad (3.54)$$

Where γ represents the absorber strength and $\epsilon(t)$ represents the absorber displacement.

Substituting Equation (3.54) into Equation (3.53) yields

$$\Delta\phi = \gamma \int_V \left\{ \int_{-\infty}^{\infty} [\delta(x-x_p - \epsilon(t)) - \delta(x-x_p)] \phi_0 \phi^\dagger e^{i\omega t} dt \right\} dx. \quad (3.55)$$

Integrating over the reactor volume yields

$$\begin{aligned} \Delta\phi(x_0, \omega) = \gamma \int_{-\infty}^{\infty} \{ & \phi(x_p + \epsilon(t)) \phi^\dagger(x_p + \epsilon(t), x_0, \omega) \\ & - \phi(x_p) \phi^\dagger(x_p, x_0, \omega) \} e^{i\omega t} dt. \end{aligned} \quad (3.56)$$

The term $\phi(x_p + \epsilon(t)) \phi^\dagger(x_p + \epsilon(t), x_0, \omega)$ may be expanded in a Taylor series which upon substitution into Equation (3.56) yields

$$\Delta\phi(x_0, \omega) = \gamma \left[\phi(x_p) \frac{\partial \phi^\dagger}{\partial x} + \phi^\dagger(x_p, x_0, \omega) \frac{\partial \phi}{\partial x} \right] \int_{-\infty}^{\infty} \epsilon(t) e^{i\omega t} dt. \quad (3.57)$$

The term $\int_{-\infty}^{\infty} \epsilon(t) e^{i\omega t} dt$ in Equation (3.57) is equal to $\epsilon(\omega)$, the Fourier transform of the absorber displacement.

Then Equation (3.57) becomes

$$\Delta\phi(x_0, \omega) = \gamma \left[\phi(x_p) \frac{\partial \phi^\dagger(x, x_0, \omega)}{\partial x} + \phi^\dagger(x_p, x_0, \omega) \frac{\partial \phi(x_p)}{\partial x} \right] \epsilon(\omega) \quad (3.58)$$

D. Extension to a Multigroup Formulation

For the purposes of extension to an n-group energy analysis, go back to Equation (3.50) and changes its parameters as follows

$$\Sigma_d = \begin{bmatrix} \Sigma_{d_1} \\ \Sigma_{d_2} \\ \vdots \\ \Sigma_{d_n} \end{bmatrix}, \quad \Delta\phi = \begin{bmatrix} \Delta\phi_1 \\ \Delta\phi_2 \\ \vdots \\ \Delta\phi_n \end{bmatrix},$$

$$\phi^\dagger = \begin{bmatrix} \phi_1^\dagger \\ \phi_2^\dagger \\ \vdots \\ \phi_n^\dagger \end{bmatrix} \quad \text{and} \quad Q = \begin{bmatrix} Q_1 \\ Q_2 \\ \vdots \\ Q_n \end{bmatrix}. \quad (3.59)$$

Then Equation (3.50) becomes

$$\int_V \sum_{i=1}^n \Sigma_{d_i} \Delta\phi_i dx = \int_V \sum_{i=1}^n Q_i \phi_i dx \quad (3.60)$$

The detector response (ΔR) can be represented as follows

$$\Delta R = (\phi^\dagger, Q). \quad (3.61)$$

Where ϕ^\dagger and Q are the adjoint function for the flux, ϕ and Q is the noise source, respectively. Both ϕ^\dagger and Q are complex quantities and can be represented as follows:

$$\begin{aligned} \phi^\dagger &= \psi + j\chi \\ Q &= Q_R + jQ_I. \end{aligned} \quad (3.62)$$

Equation (3.61) becomes

$$\Delta R = \int_{\underline{r}} [\phi^{\dagger*}]^T Q \, d\underline{r}. \quad (3.63)$$

Now, introduce Equation (3.62) into Equation (3.63)

to obtain

$$\begin{aligned} \Delta R &= \int_{\underline{r}} [\psi - j\chi]^T [Q_R + jQ_I] \, d\underline{r} \\ &= \int [\psi_1 - j\chi_1, \psi_2 - j\chi_2, \dots, \psi_n - j\chi_n] \begin{bmatrix} Q_{1R} + jQ_{1I} \\ Q_{2R} + jQ_{2I} \\ \vdots \\ Q_{nR} - Q_{nI} \end{bmatrix} \, d\underline{r} \\ &= \int_{\underline{r}} \sum_{i=1}^n (\psi_i Q_{iR} + \chi_i Q_{iI}) \, d\underline{r} + j \int_{\underline{r}} \sum_{i=1}^n (\psi_i Q_{iI} - \chi_i Q_{iR}) \, d\underline{r}. \end{aligned} \quad (3.64)$$

Where the first term and the second term from the RHS of Equation (3.64) represent the real part and the imaginary

part of the detector response respectively. Equation (3.64) could be written as follows:

$$\Delta R = \Delta R_{\text{Real}} + j\Delta R_{\text{Imag.}}$$

or

$$\Delta R = |\Delta R|e^{j\theta}. \quad (3.65)$$

where $|\Delta R|$ represents the amplitude of R and can be formulated as

$$|\Delta R| = [(\Delta R_{\text{Real}})^2 + (\Delta R_{\text{Imag.}})^2]^{1/2} \quad (3.66)$$

and θ in Equation (3.65) represents the phase of ΔR and can be formulated as

$$\theta = \tan^{-1} \frac{\Delta R_{\text{Imag.}}}{\Delta R_{\text{Real}}}.$$

Consider a two group model for an illustration.

Using the same procedure as in the one group model derivation for a nuclear parameter fluctuation will yield the two group equations stated below:

$$\begin{aligned} \nabla \cdot D_1 \nabla \Delta \phi_1 - \left[\Sigma_1 + \frac{S}{V_1} \right] \Delta \phi_1 + v \Sigma_f \left[1 - \beta \Sigma \frac{\lambda_i \beta_i}{\lambda_k + S} \right] \Delta \phi_2 \\ = -\nabla \cdot \Delta D_1 \nabla \phi_1 + \Delta \Sigma_1 \phi_1 - v \Delta \Sigma_f \left[1 - \beta + \Sigma \frac{\lambda_i \beta_i}{\lambda_i + S} \right] \phi_2 \\ = Q_1 \end{aligned} \quad (3.67)$$

$$\begin{aligned} \nabla \cdot D_2 \Delta \nabla \phi_2 - \left[\Sigma_2 + \frac{S}{V_2} \right] \Delta \phi_2 + \Sigma_{12} \Delta \phi_1 \\ = -\nabla \cdot \Delta D_2 \nabla \phi_2 + \Delta \Sigma_2 \phi_2 - \Delta \Sigma_{12} \phi_1 = Q_2. \end{aligned} \quad (3.68)$$

Use the matrix form for formulating Equations (3.67)

and (3.68) to obtain

$$\begin{bmatrix} \nabla \cdot D_1 \nabla - \Sigma_1 - \frac{S}{V_1} & \nu \Sigma_f (1 - \beta + \Sigma \frac{\beta_i \lambda_i}{\lambda_i + S}) \\ \Sigma_{12} & \nabla \cdot D_2 - \Sigma_2 - \frac{S}{V_2} \end{bmatrix} \begin{bmatrix} \Delta \phi_1 \\ \Delta \phi_2 \end{bmatrix} = \begin{bmatrix} Q_1 \\ Q_2 \end{bmatrix}. \quad (3.69)$$

Equation (3.69) can be written in this form

$$L \Delta \phi = Q \quad (3.70a)$$

where

$$\begin{aligned} Q &= [Q_1, Q_2]^T \\ \Delta \phi &= [\Delta \phi_1, \Delta \phi_2]^T \end{aligned} \quad (3.70b)$$

and L is the first matrix in Equation (3.69).

The corresponding adjoint equations for Equation (3.70a)

and (3.70b) are

$$L^\dagger \phi^\dagger = \Sigma_d \quad (3.71a)$$

where

$$\begin{aligned} \Sigma_d &= [\Sigma_{d_1}, \Sigma_{d_2}]^T \\ \phi^\dagger &= [\phi_1^\dagger, \phi_2^\dagger]^T \end{aligned} \quad (3.71b)$$

$$L = (L^T)^*$$

$$\phi_1^\dagger = \psi_1 + j\chi_1$$

$$\phi_2^\dagger = \psi_2 + j\chi_2. \quad (3.72)$$

Now, applying the inner product to Equation (3.70) and (3.71) yields

$$(\phi^\dagger, Q) = (\Sigma_d, \Delta\phi). \quad (3.73)$$

Then, the detector response at r_d with volume Δr to a noise source located at r_s with volume Δr_s , can be represented as

$$\Delta R = \int_{\Delta r_d} \Sigma_d^T \Delta\phi \, dr$$

$$\Delta R = \int_{\Delta r_d} [\Sigma_{d1}, \Sigma_{d2}] \begin{bmatrix} \Delta\phi_1 \\ \Delta\phi_2 \end{bmatrix} dr$$

$$\Delta R = \int_{\Delta r_d} [\Sigma_{d1} \Delta\phi_1 + \Sigma_{d2} \Delta\phi_2] dr. \quad (3.74)$$

Equation (3.74) describes the detector response due to the fluctuation of the flux.

The detector response can also be represented as

$$\begin{aligned}
\Delta R &= \int_{\Delta r_s} [\phi^{\dagger*}]^T Q \, dr \\
&= \int_{\Delta r_s} [\phi_1^{\dagger*} Q_1 + \phi_2^{\dagger*} Q_2] \, dr.
\end{aligned} \tag{3.75}$$

Introducing the equivalent to Q_1 , Q_2 from Equations (3.67) and (3.68) into Equation (3.75) yields

$$\begin{aligned}
\Delta R &= \int_{\Delta r_s} \Delta D_1 \nabla \phi_1 \nabla \phi_1^{\dagger*} \, dr + \int_{\Delta r_s} \Delta D_2 \nabla \phi_2 \nabla \phi_2^{\dagger*} \, dr \\
&+ \int_{\Delta r_s} \Delta \Sigma_1 \phi_1 \phi_1^{\dagger*} \, dr + \int_{\Delta r_s} \Delta \Sigma_2 \phi_2 \phi_2^{\dagger*} \, dr - \int_{\Delta r_s} \Delta \Sigma_{12} \phi_1 \phi_2^{\dagger*} \, dr \\
&- \int_{\Delta r_s} v \Delta \Sigma_f (1 - \beta + \Sigma \frac{\lambda_i \beta_i}{\lambda_i + S}) \phi_2 \phi_1^{\dagger*} \, dr.
\end{aligned} \tag{3.76}$$

Since the imaginary part for the adjoint flux is very small compared to the real part, it follows that Equation (3.76) can be written approximately as

$$\begin{aligned}
\Delta R &\approx \int_{\Delta r_s} \Delta D_1 \nabla \phi_1 \nabla \psi_1 \, dr + \int_{\Delta r_s} \Delta D_2 \nabla \phi_2 \nabla \psi_2 \, dr \\
&+ \int_{\Delta r_s} \Delta \Sigma_1 \phi_1 \psi_1 \, dr + \int_{\Delta r_s} \Delta \Sigma_2 \phi_2 \psi_2 \, dr - \int_{\Delta r_s} \Delta \Sigma_{12} \phi_1 \psi_2 \, dr \\
&- \int_{\Delta r_s} v \Delta \Sigma_f (1 - \beta + \Sigma \frac{\lambda_i \beta_i}{\lambda_i + S}) \phi_2 \psi_1 \, dr.
\end{aligned} \tag{3.77}$$

IV. INPUT DATA PREPARATION FOR WHIRLAWAY AND LEOPARD COMPUTER CODES

A. UTR-10 Model Used in this Work

The UTR-10 reactor is a coupled core reactor. The core tanks are open-topped rectangular chambers 5.844" (14.84 cm) x 19.938" (50.64 cm) x 58" (147.32 cm) high formed from 1/4" (0.635 cm) aluminum plate. Each tank is subdivided by 1/8" (0.3175 cm) aluminum dividers into six fuel chambers. The moderator-coolant enters the bottom of each core tank and flows upward through the fuel elements and out an overflow line located at the top of the core tank. Five graphite stringers are provided in the reflector region between the core tanks. One of the stringers is 3.75" (9.525 cm) x 3.75" (9.525) x 48" (121.92 cm) long and is located at the center of the core. The other four stringers are 1.188" (3.0175 cm) x 3.188" (8.097 cm) x 48" (121.92 cm) long and are grouped around the central stringer. Access to the stringers is provided through ports in the top shield closure.

The UTR-10 model used in this work is the upper half of the reactor where the midplane is taken as a plane of symmetry. Figure (4.1) shows the upper-half symmetric model for the UTR-10 reactor.

Figure 4.2 shows the UTR-10 U-235 loading for each fuel assembly.

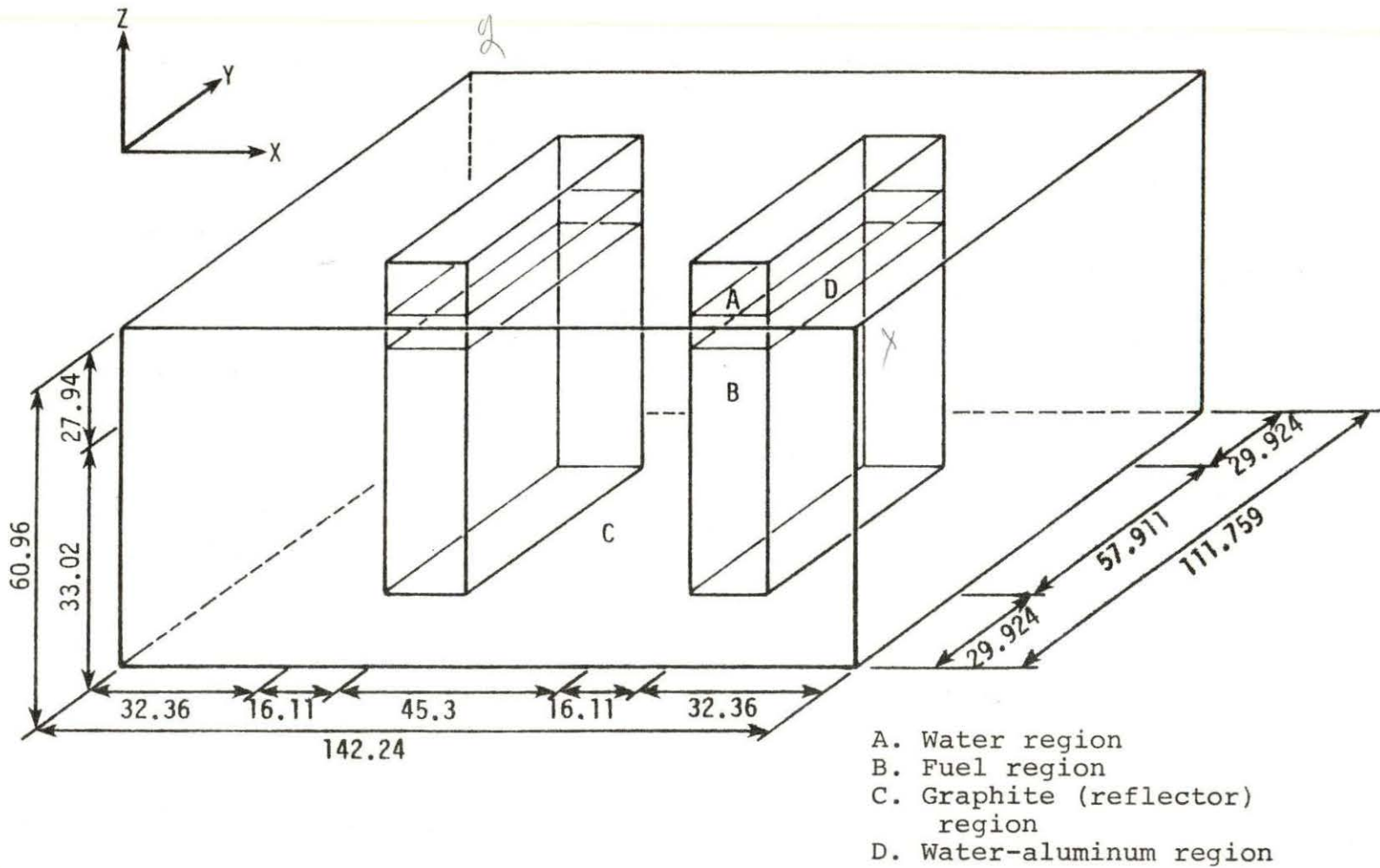


Figure 4.1. Upper half of UTR-10 reactor (all units are in centimeters)

N-1	N-2	N-3	N-4	N-5	N-6
229.13 gm	247.34 gm	261.50 gm	261.73 gm	261.56 gm	239.52 gm

S-1	S-2	S-3	S-4	S-5	S-6
196.40 gm	261.53 gm	261.90 gm	261.64 gm	261.53 gm	239.98 gm

Figure 4.2. The UTR-10 U-235 loading

Each fuel assembly may contain up to 12 fuel plates.

Figure 4.3 shows a fuel assembly cross section.

In the modeling calculation the fuel region was treated as a homogenized mixture of a UAl_4 fuel metallic matrix, water and aluminum. Figure 4.4 shows a schematic diagram for a UTR-10 fuel plate. The average mass of U-235 fuel in each fuel plate is equal to approximately 22 gm.

Table 4.1 shows the enrichment and U-235 weight in each assembly.

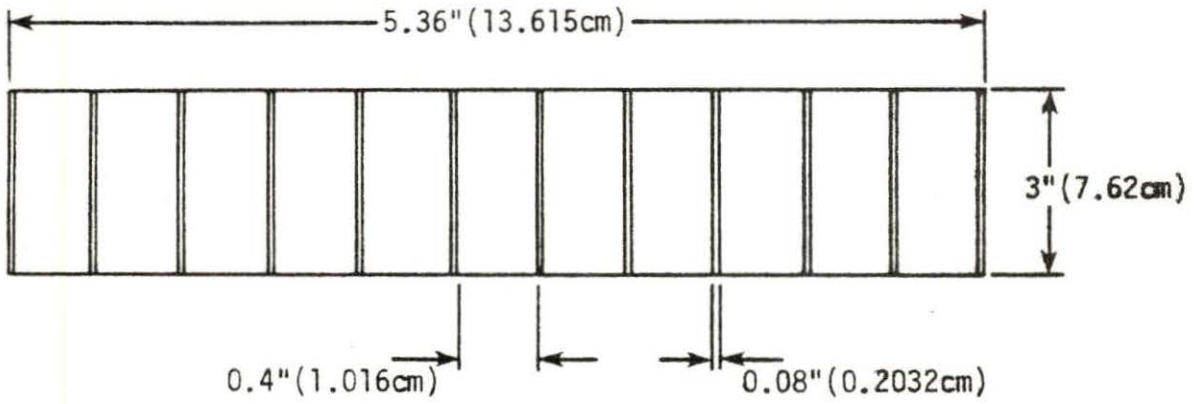


Figure 4.3. Schematic cross sectional diagram for the UTR-10 fuel assembly

Table 4.1. UTR-10 fuel enrichment and U-235 weight for each assembly

Assembly no.	Enrichment %	U-235 weight (gm)	Assembly no.	Enrichment %	U-235 weight (gm)
N-1	93.37	229.13	S-1	93.36	196.40
N-2	93.32	247.34	S-2	93.37	261.53
N-3	93.37	261.50	S-3	93.37	261.90
N-4	93.39	261.73	S-4	93.37	261.64
N-5	93.39	261.56	S-5	93.37	261.53
N-6	93.37	239.52	S-6	93.38	239.98

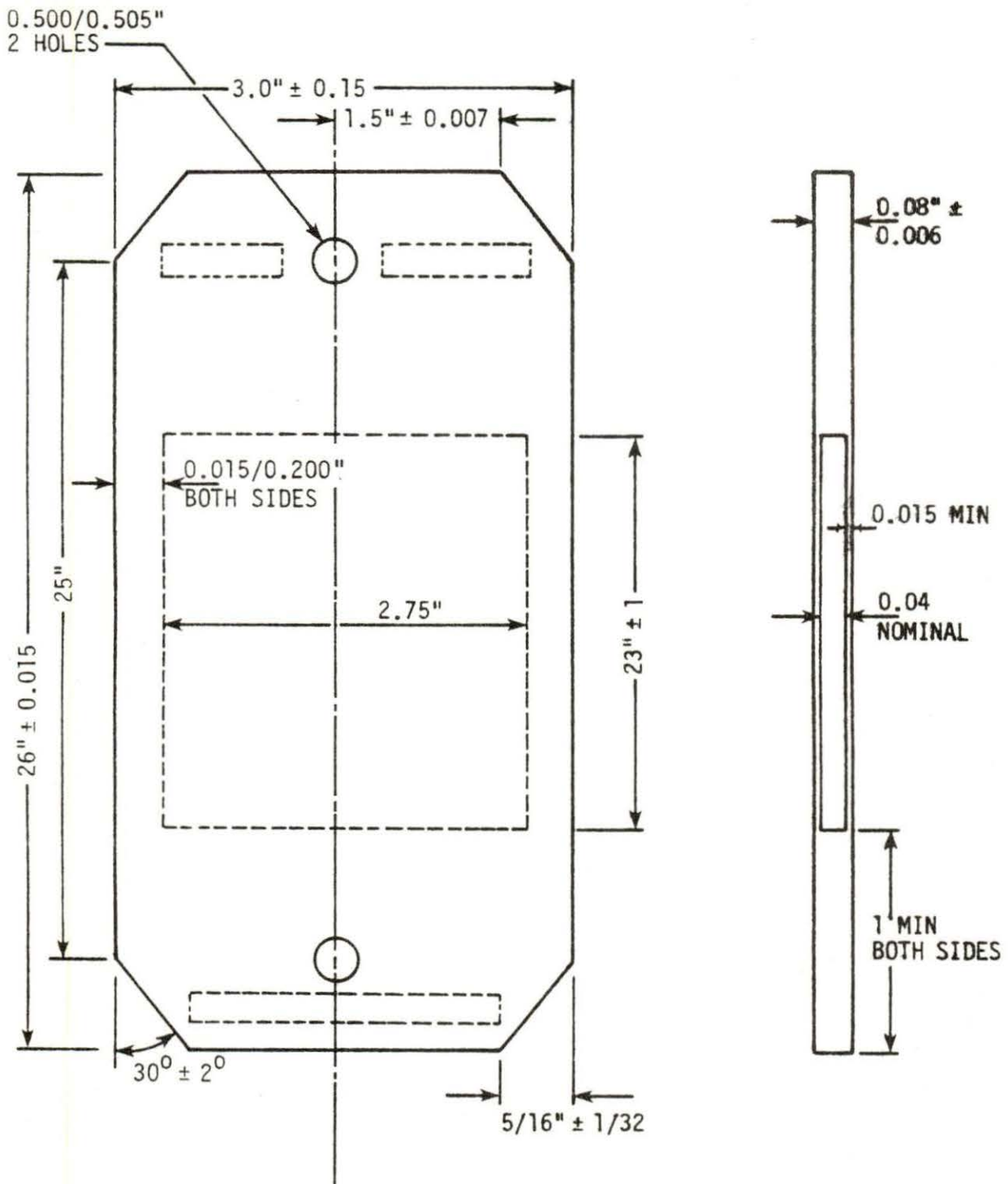


Figure 4.4. Schematic diagram for UTR-10 fuel plate (all units are in inches)

To increase the detail of the flux and adjoint flux calculation, the macroscopic parameters were calculated for each individual fuel assembly using the cross section code LEOPARD. The 1.5" (3.81 cm) top of each fuel assembly was treated as a mixture of water and aluminum without fuel. In the next section more detail is given on the actual preparation of the input data for LEOPARD.

B. Description of the Input Data for LEOPARD

LEOPARD (2) is a computer program which determines the fast and thermal nuclear parameters. LEOPARD requires only the most basic input data. The reactor geometry, compositions and temperatures are supplied by the user.

The input data for LEOPARD for the fuel regions were based on the volume fraction of U-235 and U-238 for each assembly in the reactor. As pointed out before, the fuel region was treated as a homogenized mixture of UAl_4 fuel matrix, water and aluminum. It was assumed that the core tank was part of the fuel region and it was included in the calculation by including it in the nonlattice fraction.

To illustrate the determination of the nonlattice fraction, consider the water-aluminum region shown in Figure 4.5 which is the top part of the fuel region.

Figure 4.5 does not show the extent of the fuel plates,

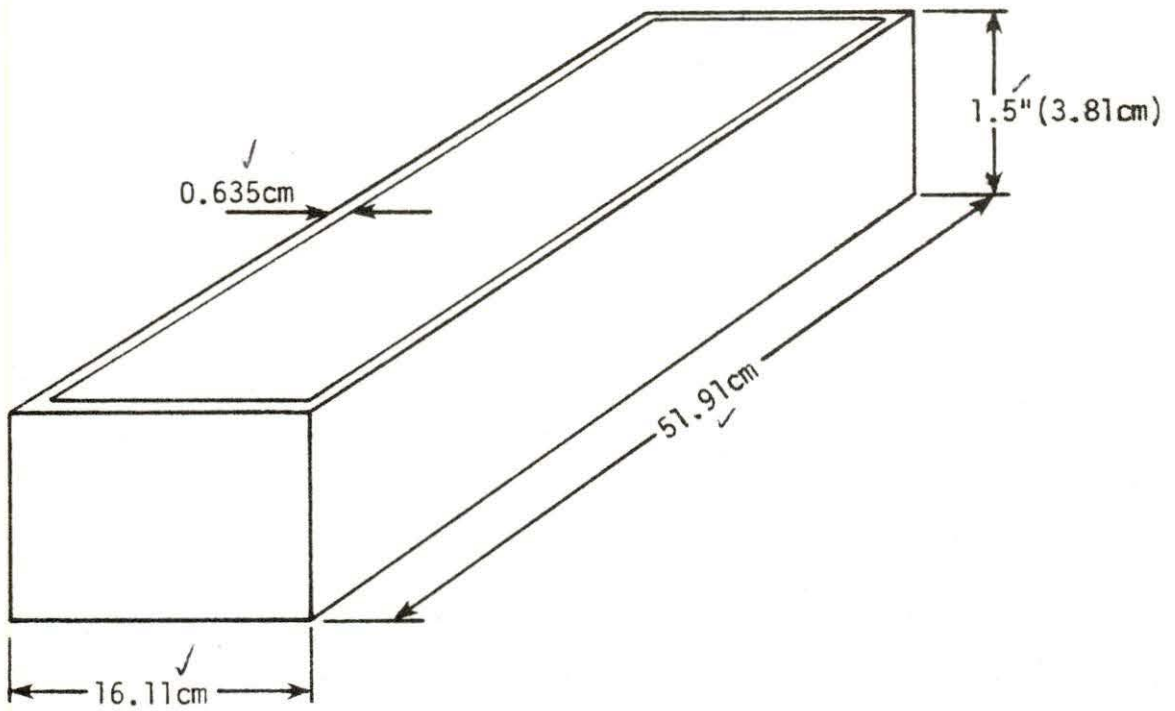


Figure 4.5. Schematic diagram for the general shape of water-aluminum region

the bolts and spacers and the divider between each fuel plate.

The following calculations are required to determine the nonlattice fraction

$$\begin{aligned} \text{Total box volume} &= 3.81 \times 51.91 \times 16.11 \\ &= 3186.19 \text{ cm}^3 \end{aligned}$$

$$\begin{aligned} \text{Inside box volume} &= 3.81 \times 50.65 \times 14.83 \\ &= 2861.71 \text{ cm}^3 \end{aligned}$$

$$\text{Total volume} - \text{Inside volume} = 324.48 \text{ cm}^3$$

= The contribution of the core tank to the total volume

The volume of the bolts

$$= 11 \frac{\pi (0.75)^2}{4} (2.54)^2 (0.4) (2.54) \times 6 = 191.12 \text{ cm}^3$$

$$\begin{aligned} \text{Volume of dividers} &= 14.45 \times 0.32 \times 3.81 \times 7 \\ &= 123.32 \text{ cm}^3 \end{aligned}$$

Hence, the nonlattice fraction is

$$\frac{324.48 + 191.12 + 123.32}{3186.19} = \frac{638.92}{3186.19} = 0.2005.$$

In order to calculate the volume fraction of the U-235 and U-238, the following procedures were used:

1. Number of atoms in a fuel plate

$$= \frac{\text{Uranium weight}}{\text{Atomic weight}} \times \text{Avogadro's number}$$

2. Atom density = $\frac{\text{No. of atoms}}{\text{cm}^3 \text{ of alloy}}$

$$3. \text{ Volume fraction} = \text{Atom density} \times 10^{-24} .$$

Using assembly Number 1 in the north tank as an example, the weight of Uranium-235 in this assembly is equal to 229.13 gm.

Now, the volume of alloy

$$= 12 \times 23 \times 0.04 \times 2.75 \times (2.54)^3 = 497.51 \text{ cm}^3 .$$

Number of atoms of U-235

$$= \frac{229.13}{235} \times 6.022045 \times 10^{23}$$

$$= 5.871622 \times 10^{23} .$$

$$\text{Atom density} = \frac{5.871622 \times 10^{23}}{497.51} = 0.0011802 \times 10^{24} / \text{cm}^3 .$$

Then, the U-235 volume fraction in this assembly is equal to (0.0011802).

To calculate the volume fraction for U-238, the enrichment in each assembly is known, so that the U-238 weight in each assembly can be determined and from this can be calculated by following the same procedure explained in the example above. Table 4.2 shows the volume fractions for U-235 and U-238 in each assembly in the UTR-10 reactor. Note that for fuel plate type elements the U-235 and U-238 are entered as outlined above rather than as trace elements as described in the LEOPARD manual.

Using assembly Number 1 from the north core as an

Table 4.2. Volume fractions in each assembly in UTR-10 reactor

Assembly number	Enrichment %	U-235 weight (gm)	Volume fraction	U-238 weight (gm)	Volume fraction $\times 10^4$
N-1	93.37	229.13	0.0011802	16.270	0.8275
N-2	93.32	247.34	0.0012740	17.705	0.9005
N-3	93.37	261.50	0.0013470	18.568	0.9443
N-4	93.39	261.73	0.0013481	18.525	0.9422
N-5	93.39	261.56	0.0013472	18.513	0.9415
N-6	93.37	239.52	0.0012337	17.008	0.8650
S-1	93.36	196.40	0.0010116	13.968	0.7104
S-2	93.37	261.53	0.0013471	18.571	0.9445
S-3	93.37	261.90	0.0013490	18.597	0.9458
S-4	93.37	261.64	0.0013477	18.578	0.9448
S-5	93.37	261.53	0.0013471	18.571	0.9445
S-6	93.38	239.98	0.0012361	17.013	0.8652

example, the following input data are used in LEOPARD:

1. The title card (80 columns) and is printed on every page of the output.
2. Option - meanings of the various options are as follows:

	<u>Entry</u>	<u>Column</u>
A. Change case	0	3
Reference case	1*	
B. Temperatures in °F	0*	6
Temperatures in °R	1	
Temperatures in °K	2	
Temperatures in °C	3	
C. Lengths in c	0	9
Lengths in inches	1*	
D. Square cell	0	12
Hexagonal cell	1	
Slab cell	2*	
E. Search for L-238	0	15
Use input L-238	1*	
F. Dimensions are hot	0	18
Dimensions are cold	1*	
G. σ_{rem} fitted for element	1*	21
N. No lifetime steps	0*	42
Some lifetime steps	1	
Q. B_M^2 criticality search	0	50
Thermal poison search	-1	
No search	-2*	
Poison search	+t	
R. Omit	0*	54
Adjust geometric buckling with burn up	+1	

* The options used to calculate the UTR-10 nuclear parameters.

The other input data for the N-1 assembly are as follows:

Volume fractions:

<u>Index</u>	<u>Pellet</u>	<u>Clad</u>	<u>Moderator</u>	<u>Extra</u>
9	0.975	1.0	0.0	1.0
18	0.0011802	0.0	0.0	0.0
20	0.000082747	0.0	0.0	0.0
100	0.0	0.0	1.0	0.0
777	0.0	0.0	0.0	0.0

Trace elements:

777	0.0	0.0	0.0	0.0
-----	-----	-----	-----	-----

Temperatures, buckling, and peaking factor:

90.0	90.0	90.0	0.00194	1.0
------	------	------	---------	-----

Radii and nonlattice fraction:

0.02	0.04	0.48		0.1486
------	------	------	--	--------

H₂O pressure:

14.7

C. LEOPARD Output Which is Used
As Input Data to
the WHIRLAWAY Code

The output data from LEOPARD consist of the nuclear parameter shown in Table 4.3. These were used as part of the input to the neutron diffusion code WHIRLAWAY which is discussed in the following section.

Table 4.3. LEOPARD output

Column	Region	21-26	27-32	33-40	41-48	49-56	57-64	65-72
		D_1	D_2	Σ_{R_1}	Σ_{a_1}	Σ_{a_2}	$\nu\Sigma_{f_1}$	$\nu\Sigma_{f_2}$
W&Al ^a		1.4396	0.2296	0.033042	0.000767	0.016313	0.0	0.0
W ^a		1.3226	0.1552	0.048367	0.000797	0.018785	0.0	0.0
G ^a		1.1528	0.9925	0.002867	0.532 E-8	0.305 E-3	0.0	0.0
N-1		1.4214	0.2265	0.034121	0.001973	0.052734	0.001887	0.077098
N-2		1.4313	0.2272	0.034050	0.002065	0.055204	0.002033	0.082362
N-3		1.4212	0.2277	0.033995	0.002137	0.057093	0.002147	0.086390
N-4		1.4212	0.2277	0.033995	0.002138	0.057123	0.002150	0.086455
N-5		1.4212	0.2277	0.033995	0.002137	0.057101	0.002148	0.086407
N-6		1.4213	0.2269	0.034081	0.002025	0.054148	0.001971	0.080114
S-1		1.4216	0.2253	0.034249	0.001805	0.048179	0.001621	0.067384
S-2		1.4212	0.2277	0.033995	0.002137	0.057097	0.002147	0.086399
S-3		1.4212	0.2277	0.033994	0.002139	0.057146	0.002149	0.086503
S-4		1.4212	0.2277	0.033995	0.002137	0.057112	0.002149	0.086429
S-5		1.4212	0.2277	0.033995	0.002137	0.057097	0.002147	0.086399
S-6		1.4213	0.2269	0.034079	0.002028	0.054211	0.001972	0.080246

^aW&Al, W, and G are the abbreviations of water and aluminum region, water region, and graphite region, respectively.

D. WHIRLAWAY Input Data

WHIRLAWAY (15) is a three-dimensional program in slab geometry and two groups. 12,750 points may be treated. Adjoint information may be obtained, but control rod boundary conditions are not available. The maximum number of iterations is 300. The speed of calculation does depend on the number of regions. For example, a certain one-region problem took about 10% longer when the reactor was subdivided into 20 regions.

The nuclear parameters used as input data to WHIRLAWAY-H were prepared by using the LEOPARD computer code. The instructions for writing the input data to WHIRLAWAY-H are explained as follows:

1. Title card (20A4): is the title of the problem
2. Tape control card (2I5)

To reduce the cost of running this computer code, it is better to use two tapes for storing the outputs. By using the tapes one can save at least half of the run cost or more. For the first run put NRTAPE=0 and NNTAPE=1. In this, the initiation of the calculation starts using the program supplied first flux estimates and stores the converged flux solutions on tape #11. For the next run, use the data that are already stored on tape #11 as initial flux values. In this case NRTAPE=1 and NNTAPE=2 are used to read the flux

estimates from tape Number 11 and to write them on tape Number 12 and so on. If it is desired to keep several outputs on tape the file number and the data set name in the job control cards that belong to the unit that the data are going to be stored on should be changed for each run.

The following is the tape control specification:

NRTAPE = 0 Use the initial flux distribution provided by the code

= 1 Read the initial fluxes from tape #11

= 2 Read the initial fluxes from tape #12

NNTAPE = 0 The converged fluxes are not written on any tape

= 1 The converged fluxes are written on tape #11

= 2 The converged fluxes are written on tape #12

3. Adjoint source specification card (I10, 2F10.0, I10)

NNORM = 1 The flux and/or adjoint flux are normalized with respect to the maximum flux or adjoint flux.

= 0 The flux and adjoint flux are normalized to the total fission source

SIGMD1: The fast adjoint source, usually the detector cross section for fast group, cm^{-1} (used as zero for both the regular and the adjoint flux calculation for a thermal neutron detector).

SIGMD2: The thermal adjoint source, usually the detector cross section for thermal group, cm^{-1} (used zero for the regular flux calculation and one for the adjoint flux calculation).

NGEMW: The external neutron source region index number. This indicates the perturbation region index number and it does not do anything to the calculation. If no external source is used, put NGEMW equal to zero.

4. Graph plotting control cards (24I3).

NPLOTI \leq 3: Number of curves to be plotted in X-direction.

NASJ1, NASK1, NASJ2, NASK2, NASJ3, NASK3: The first two specify the mesh index of the Y-plane and the mesh index of the Z-plane for the first curve in X-direction. The following four numbers specify the second and third curve in the X-direction.

NPLOTJ \leq 3: Number of curves to be plotted in Y-direction.

NAK1, NAI1, NAK2, NAI2, NAK3, NAI3: These six mesh indices specify the three curves in the Y-direction.

NPLOTK \leq 3: Number of curves to be plotted in Z-direction.

NNAI1, NNAJ1, NNAI2, NNAJ2, NNAI3, NNAJ3: The six mesh indices specify the three curves in the Z-direction.

5. The graph size card (2F10.0).

XSIZE: The graph size in inches for X-axis

YSize: The graph size in inches for Y-axis

6. The heading cards \leq 9: These cards provide the title and the information needed in the upper right corner of the plots.

If no graph plotting is required, discard the graph plotting control card, the graph size card and the heading cards. Put two blank cards after the adjunct source specification card.

7. The control card (3I3, E9.5, 11I2, 4E6.3, E8.5)

IMAX \leq 999: Total number of mesh points in the X-direction

JMAX \leq 999: Total number of mesh points in the Y-direction

KMAX \leq 999: Total number of mesh points in the Z-direction

NORM FACTOR: Usually use 1.0 (do not use 0.0)

GI: Geometrical indicator. This number is just to indicate the detector region and it does not do anything with the calculation.

SI=1 Source calculation is applied

=0 Source calculation is skipped

AI=1 Adjoint flux and flux-adjoint flux regional integrals are calculated

=0 Adjoint calculation is skipped

FI: Not used in the calculation, but usually put 1 (do not use zero)

CI=0 The total λ convergence criterion is used to stop the calculation when

$$\left| \frac{\lambda_n - 10}{\lambda_n} - 1 \right| < \epsilon \quad (4.1)$$

where n is the iteration number and ϵ is the convergence criterion.

=+1 The total λ convergence criterion and the flux convergence criterion are both used, the calculation stops when the above condition is met, as well as the flux convergence condition

$$\left| \frac{\phi_n}{\phi_{n+1}} - 1 \right| < \epsilon \quad (4.2)$$

where ϕ_n is the flux at a point at iteration n and ϕ_{n+1} is the flux at the same point at iteration $n+1$. For the adjoint calculation, only the flux convergence condition is tested, it is given by

$$\frac{\rho_{\max} - \rho_{\min}}{\frac{1}{2}(\rho_{\max} + \rho_{\min})} < \epsilon \quad (4.3)$$

where $\rho = \phi_n / \phi_{n+1}$

= -1 The point $-\lambda$ convergence criterion and the flux convergence criterion are both used. The calculation stops when the flux condition in Equation 4.2 is met, as well as the point $-\lambda$ convergence condition

$$\frac{\lambda_{\text{pt}}^{\max} - \lambda_{\text{pt}}^{\min}}{\lambda} < \epsilon \quad (4.4)$$

where $\lambda_{\text{pt}}^{\max}$ and $\lambda_{\text{pt}}^{\min}$ are the maximum and minimum values of λ , respectively. If a problem has not reached convergence after 300 iterations, it is automatically terminated by the code.

LB=0 Left boundary is a zero flux boundary

=1 Left boundary is a symmetry boundary

RB=0 Right boundary is a zero flux boundary

=1 Right boundary is a symmetry boundary

IB,OB,BB,TB: Specify the "in", "out", bottom and top boundary conditions as described in LB and RB.

Note that in the symmetry boundary condition, one should provide a double interval for the second mesh point only because the code, in this case, will consider the midpoint between the first mesh value and the second mesh value as its

first mesh value. For example, if the first mesh value is zero and the second mesh value is 1 cm the code will consider 0.5 cm as its first mesh value. So, if 1 cm is the interval between the first and the second mesh point the user should provide 2 cm as the second mesh value and will be considered as 1 cm by the code. Figure 4.6 shows a three-dimensional diagram use in WHIRLAWAY.

χ_1 : Fraction of neutrons produced from fission that are born in group 1

χ_2 : Fraction of neutrons produced from fission that are born in group 2

β_1 : Extrapolated Liebmann coefficient for group 1

= 0 β_1 computed by the code by the following empirical formula

$$\beta + 2 - \sqrt{2} \left| \left(\frac{\pi}{P} \right)^2 + \left(\frac{\pi}{9} \right)^2 + \left(\frac{\pi}{r} \right)^2 \right|^{1/2} \quad (4.5)$$

where P, 9 and r are the number of mesh increments in the X, Y and Z-directions, respectively. If one of the opposite surfaces is a symmetry boundary, the corresponding number of mesh increments is doubled. If both opposite surfaces are symmetry boundaries, the corresponding number of mesh increments is made ∞ .

= 1 β_1 provided by the user

β_2 : Extrapolated Liebmann coefficient for group 2

= 0 β_2 computed by the code

= 1 β_2 provided by the user

If a problem has not converged after 150 iterations, a new β is calculated by

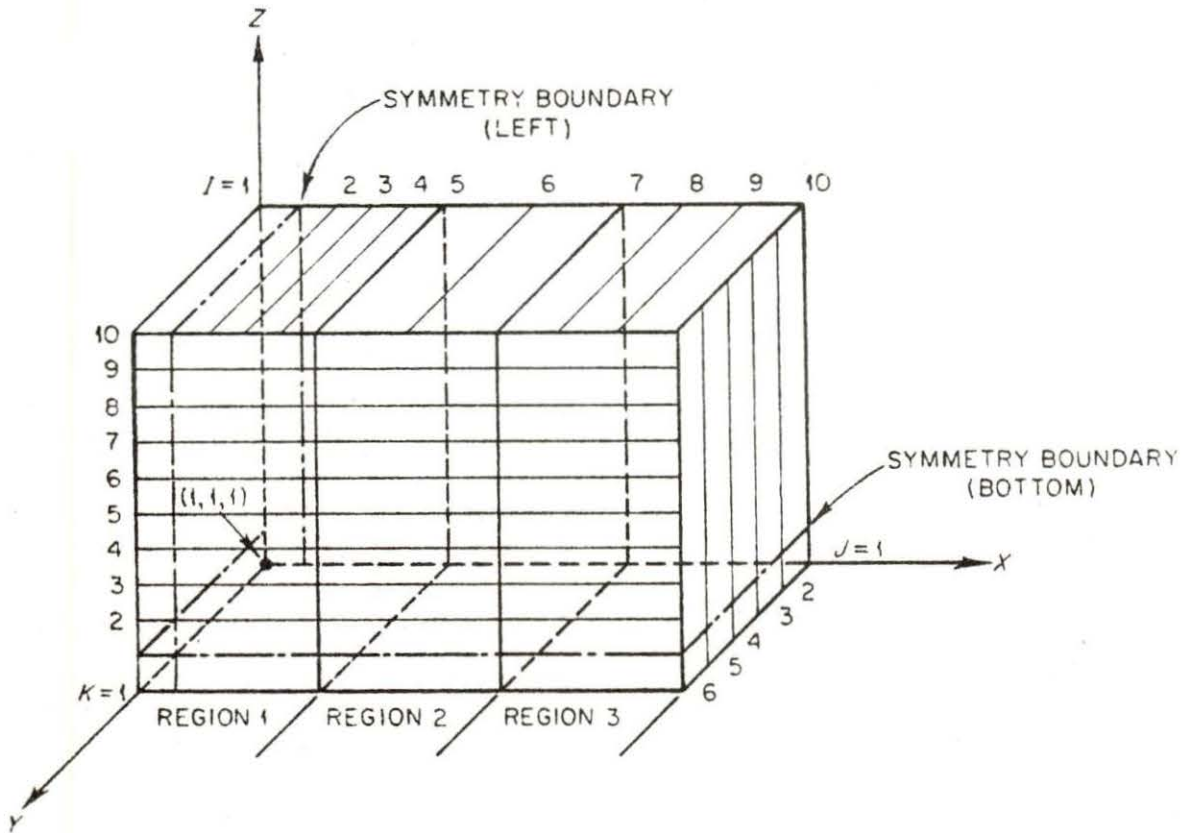


Figure 4.6. Schematic diagram of the three-dimensional cube used in WHIRLAWAY

$$\beta_{\text{new}} = \frac{\beta_{\text{old}} + 1}{2} \quad (4.6)$$

ϵ : The value for convergence criterion

8. Mesh specification cards: Described below are the three types of cards required to specify the mesh:
- (1) cards giving the ΔX 's and I numbers (mesh point),
 - (2) cards giving the ΔY 's and j numbers (mesh point),
 - (3) cards giving the ΔZ 's and K numbers (mesh point).
1. In columns 1-6 and 7-9, 10-15 and 16-18, etc., supply a value of ΔX (E6.3) and the value of I(I3) up to that which this X applies, going from left to right of the mesh. Use as many cards as needed, with each card, except possibly the last card, being completely filled through column 72. The last number on these cards is equal to IMAX.
 2. In columns 1-6 and 7-9, 10-15 and 16-18, etc., supply a value of ΔY (E6.3) and the value of j(I3) up to which this Y applies, going from "in" to "out" of the mesh. The last number on these cards is equal to JMAX.
 3. In columns 1-6 and 7-9, 10-15 and 16-18, etc., supply a value of ΔZ (E6.3) and the value of K(I3) up to which this ΔZ applies, going from bottom to top of the mesh. The last number on these cards is equal to KMAX.
9. Region specification cards: The regions are specified as parallelepipeds, with each card completely specifying one region, for as many regions as are needed to fill the mesh. The region-specification cards may be in any order. However, the regions must be numbered consecutively. One card with the number 99 punched in columns 1 and 2 must follow the last region-specification card.

Columns 1-2, RG (I2)

Region number

Columns 3-5, I1(I3)

Left I coordinate of the region

Columns 6-8, I2(I3)	Right I coordinate of the region
Columns 9-11, J1(I3)	"In" j coordinate of the region
Columns 12-14, J2(I3)	"Out" j coordinate of the region
Columns 15-17, K1(I3)	Bottom K coordinate of the region
Columns 18-20, K2(I3)	Top K coordinate of the region
Columns 21-26, D1(E6.3)	Group 1 diffusion coefficient
Columns 27-32, D2(E6.3)	Group 2 diffusion coefficient
Columns 33-40, Σ_{R_1} (E8.5)	Group 1 macroscopic removal cross section
Columns 41-48, Σ_{A_1} (E8.5)	Group 1 macroscopic absorption cross section
Columns 49-56, Σ_{A_2} (E8.5)	Group 2 macroscopic absorption cross section
Columns 57-64, $\nu\Sigma_{f1}$ (E8.5)	Group 1, ν times the macroscopic fission cross section
Columns 65-72, $\mu\Sigma_{f2}$ (E8.5)	Group 2, ν times the macroscopic fission cross section

E. WHIRLAWAY Output Description

WHIRLAWAY output consists of the following items:

1. Title (printed in every page of the output)
2. Reactor specifications
3. Mesh specifications
4. Dimension specifications

5. Region specifications
6. The values of the extrapolated Liebmann coefficients
7. Flux convergence, point λ convergence, total $-\lambda$ convergence, total residue, and λ (labeled NU-CRITICAL) at every tenth iteration. The total residue is calculated as the square root of the sum of the squares of the residues (summed over all points and groups) divided by the total source.
8. The normalized flux values for each group at each mesh point.
9. A neutron-balance list calculated from the printed-out fluxes.
10. A summary of the region-integrated group absorptions and the region volumes.
11. The source density at each octant of each internal mesh point.
12. A summary of convergence levels for the adjoint calculation.
13. The normalized adjoint-flux values at each mesh point.
14. The flux times the adjoint-flux region integrals and the region integrals of the dot products of the gradients of the flux and the adjoint flux.

For one region, the printout would be as follows:

REG PHI(1) x PHI(K)* PHI(2) x PHI(K)* DELPHI(K) x DELPHI(K)*

$$\int \phi_1 \phi_1^\dagger d\underline{r} \qquad \int \phi_2 \phi_1^\dagger d\underline{r} \qquad \int \nabla \phi_1 \nabla \phi_1^\dagger d\underline{r} \qquad k=1,2$$

$$\int \phi_1 \phi_2^\dagger d\underline{r} \qquad \int \phi_2 \phi_2^\dagger d\underline{r} \qquad \int \nabla \phi_2 \nabla \phi_2^\dagger d\underline{r}$$

15. The plots for fluxes and/or adjoint fluxes distribution along X, Y, or Z-direction.

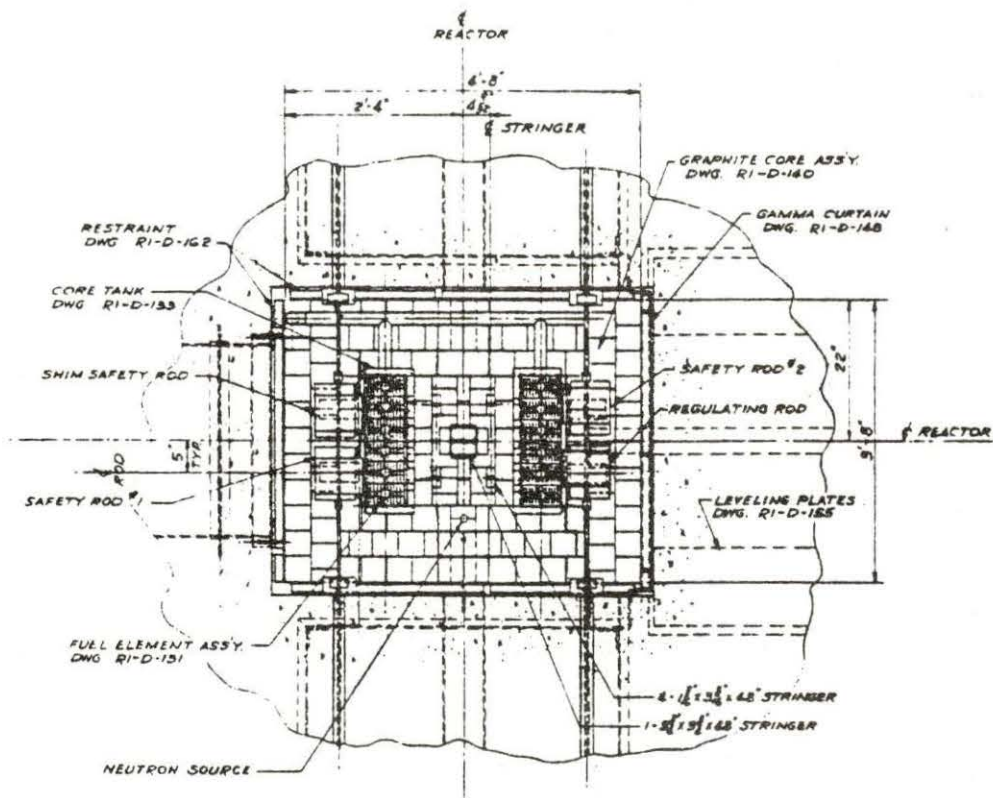
V. PROCEDURES AND RESULTS

A. K_{eff} Search

The calculation of the adjoint flux and the K_{eff} search have been done in this work by using the three-dimensional computer code WHIRLAWAY. The upper half symmetry of the UTR-10 reactor has been used in the calculation of the flux and the adjoint flux distribution, 11340 total mesh points were used in the model, distributed as 35 mesh points along the X-axis, 27 mesh points along the Y-axis and 12 mesh points along the Z-axis. Figure 5.1 shows a top view of the UTR-10 reactor. Figure 5.2 shows some mesh lines in the X and Y plane to explain the absorber and detector regions (positions). Table 5.1 shows the mesh intervals in the X, Y, and Z-directions. A number of computer runs were made to determine the change in K_{eff} for a number of reactor changes including the effect of removal of a fuel plate and the insertion of neutron detectors and an absorber. The purpose of these calculations was to obtain a reactor model having a K_{eff} of unity with detectors and absorbers inserted.

Basically the K_{eff} search was done as follows:

1. The computer code WHIRLAWAY was run for the UTR-10 reactor model without the noise source and with no change in the core structure to find $K_{eff} = 1.03436$. Figure 5.6 shows the fast and thermal flux



PLAN-CORE AREA

Figure 5.1. UTR-10 reactor (top view of core area)

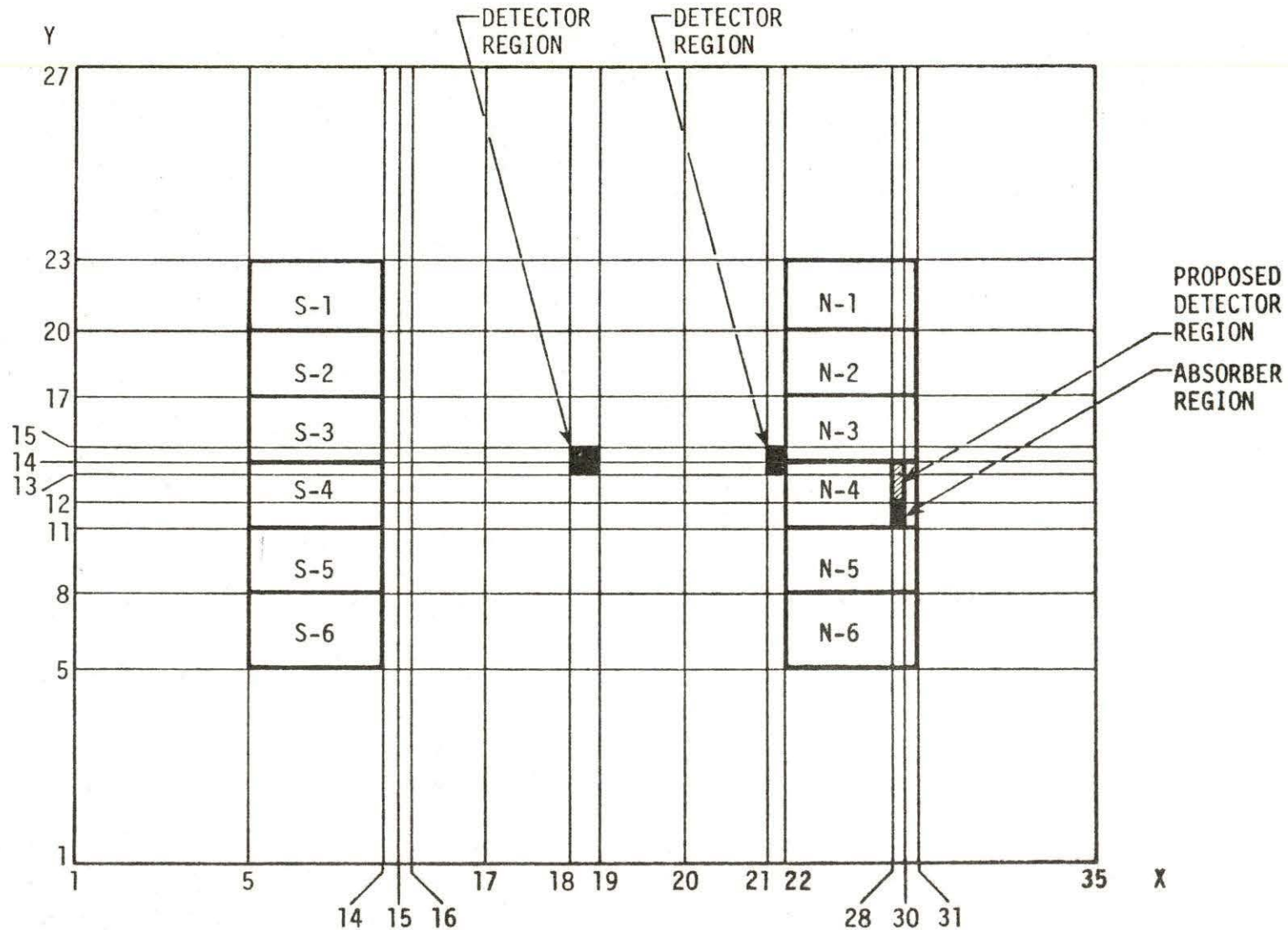


Figure 5.2. Mesh lines in the X and Y plane which define the detector and absorber regions

Table 5.1. Mesh intervals in X, Y, and Z directions

Mesh point #	X-axis cm	Y-axis cm	Z-axis cm
1	0.0	0	0
2	1.0	1	8.0
3	14.5	10.0	4.0
4	14.5	10.0	4.5
5	2.36	8.924	4.36
6	2.565	2.652	4.35
7	0.609	3.0	4.0
8	0.609	3.0	4.0
9	3.5	2.652	3.81
10	3.5	3.0	3.94
11	3.471	3.0	12.0
12	0.609	3.576	12.0
13	0.609	3.576	
14	0.635	1.5	
15	1.3	1.5	
16	2.0	3.576	
17	8.925	3.576	
18	8.925	2.652	
19	3.0	3.0	
20	9.575	3.0	
21	9.575	2.652	
22	2.0	3.0	
23	0.635	3.0	
24	0.609	8.924	
25	0.609	10.0	
26	3.471	10.0	
27	3.5	1.0	
28	3.5		
29	0.609		
30	0.609		
31	2.565		
32	2.36		
33	14.5		
34	14.5		
35	1.0		

distribution along the X-axis with $Y = 55.88$ cm and $Z = 0$ cm (at the symmetry plane). This was treated as a reference case.

2. The code was run again taking the third fuel plate from the outside of assembly N-4 to find $K_{\text{eff}} = 1.03153$. This gives a fuel plate reactivity worth of approximately 43.5¢. Figure 5.7 shows the fast and thermal flux distribution along the X-axis at $Y = 54.38$ cm and $Z = 0$ cm for this case. This plane passes through the region where the plate was removed.
3. The code was then run for the case with the thermal macroscopic absorption cross section in both cores increased using $\Sigma_p = 0.001917 \text{ cm}^{-1}$ to find $K_{\text{eff}} = 1.00161$. This gives approximately 25¢ away from criticality (i.e., $K_{\text{eff}} = 1$). Figure 5.3 shows a two-dimensional plot for the thermal flux distribution at the symmetry plane for this case.
4. The code was then run with the absorber region (representing the noise source) poisoned making $\Sigma'_p = 0.022108 \text{ cm}^{-1}$. This reduced K_{eff} to 1.00063. This gives an absorber reactivity worth approximately equal to 15¢. Figure A.1 shows the location of the absorber in the assembly N-4. Figure 5.8

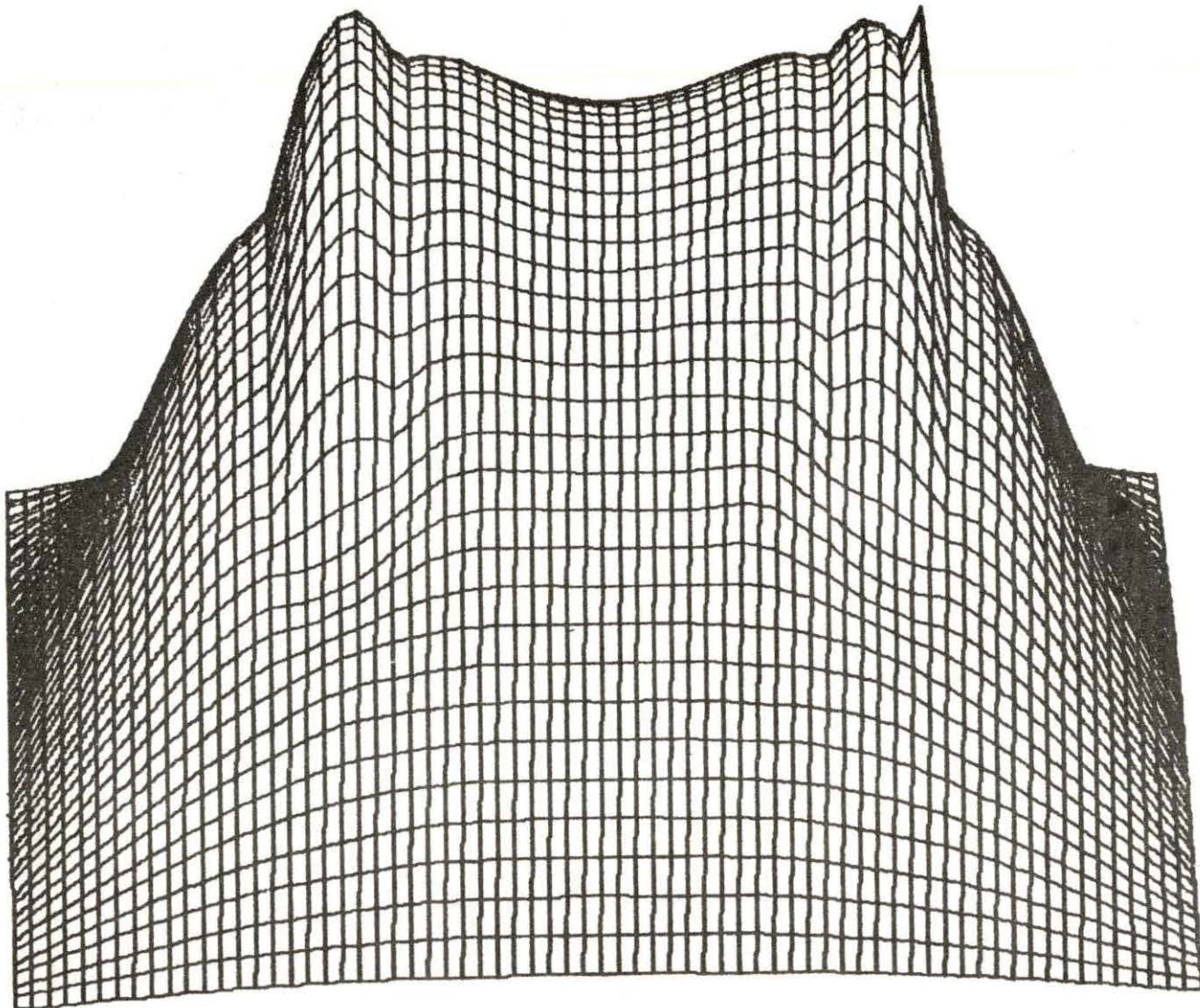


Figure 5.3. Two-dimensional plot for the UTR-10 reactor thermal flux distribution at $Z = 0$ cm, fuel plate from assembly N-4 is removed and both cores are poisoned with $\Sigma_p = 0.001917 \text{ cm}^{-1}$

shows the fast and thermal flux distribution along the X-axis with $Y = 50.804$ cm and $Z = 0$ cm for this case. This plane passes through the absorber region.

5. The code was then run for the detector region in the central stringer location poisoned using $\Sigma_p = 0.036129$ cm⁻¹ to find $K_{\text{eff}} = 1.00002$. This gives a detector worth approximately equal to 9.5¢. The size of this detector region was taken as 3 cm x 3 cm x 24 cm, which corresponds to the size of the detector to be used. Figure 5.9 shows the fast and thermal flux distribution through the detector region along the X-axis with $Y = 55.88$ cm and $Z = 0$ cm. Figure 5.4 shows a two-dimensional plot for the thermal flux distribution at the symmetry plane.
6. The code was then run, increasing the thermal macroscopic absorption cross section of a detector region located beside the north core as shown in Figure 5.2 by $\Sigma_p = 0.0315$ cm⁻¹ to find $K_{\text{eff}} = 1.00002$. This gives a detector worth approximately equal to 9.5¢. The size of this detector region was taken as 2 cm x 3 cm x 24 cm. Figure 5.10 shows the fast and thermal flux distribution along the X-axis with $Y = 54.38$ cm and $Z = 0$ cm. Figure 5.5 shows a two-dimensional plot for the thermal flux distribution

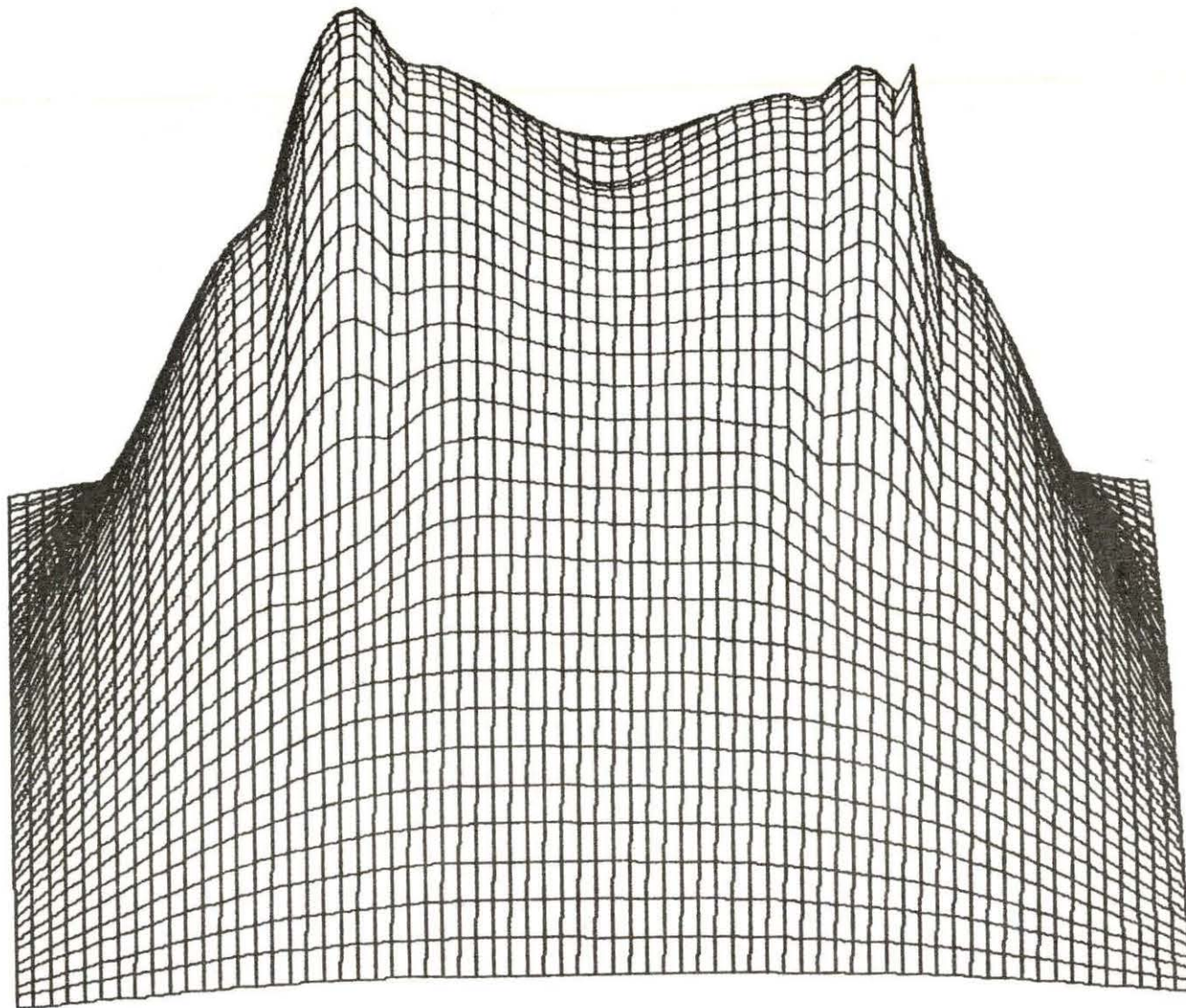


Figure 5.4. Two-dimensional plot for the UTR-10 reactor thermal flux distribution at $Z = 0$ cm with the detector region at the central stringer poisoned with $\Sigma_p = 0.036129 \text{ cm}^{-1}$

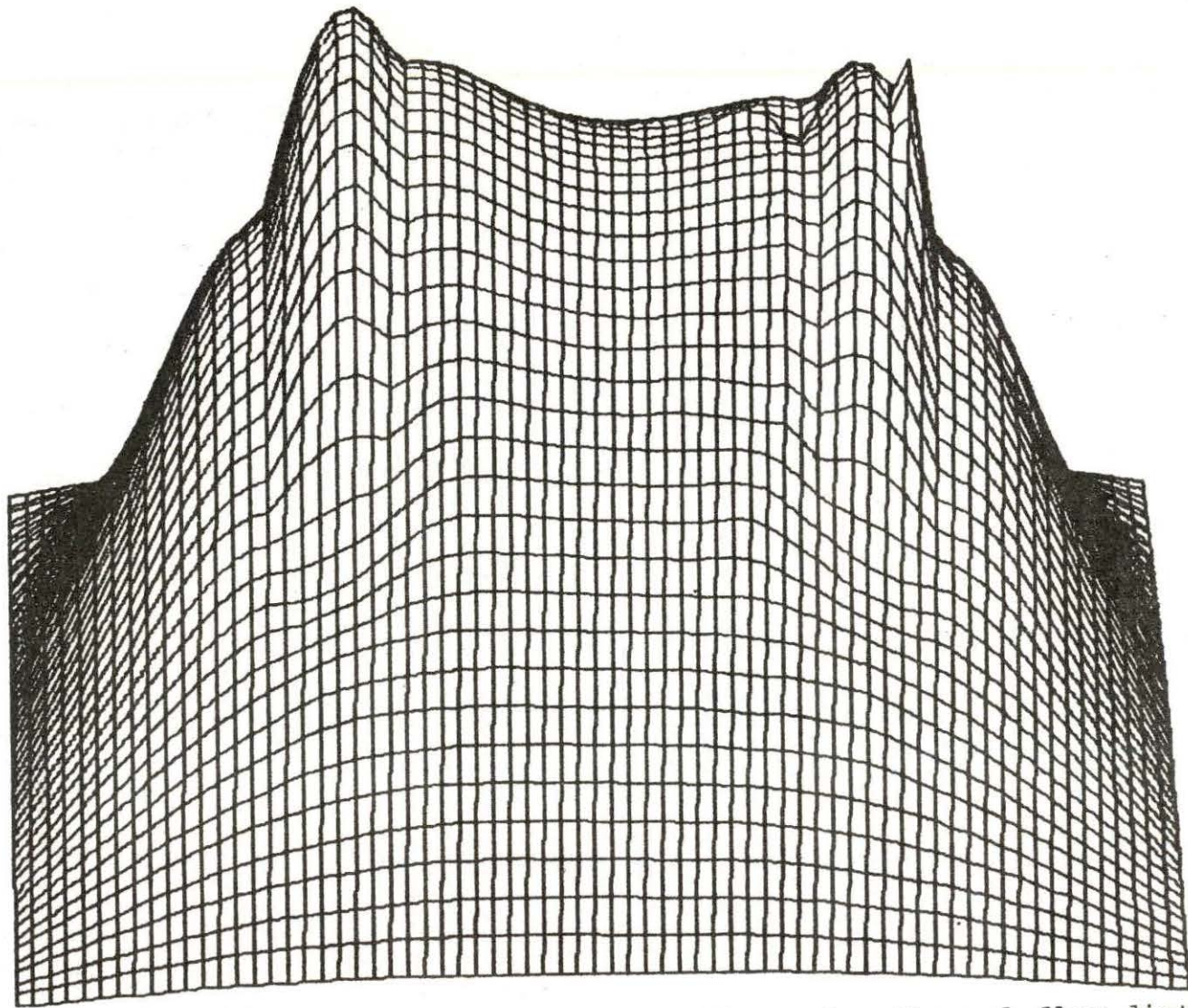


Figure 5.5. Two-dimensional plot for the UTR-10 reactor thermal flux distribution at $Z = 0$ cm, with the detector region beside the north core poisoned with $\Sigma_p = 0.0315 \text{ cm}^{-1}$

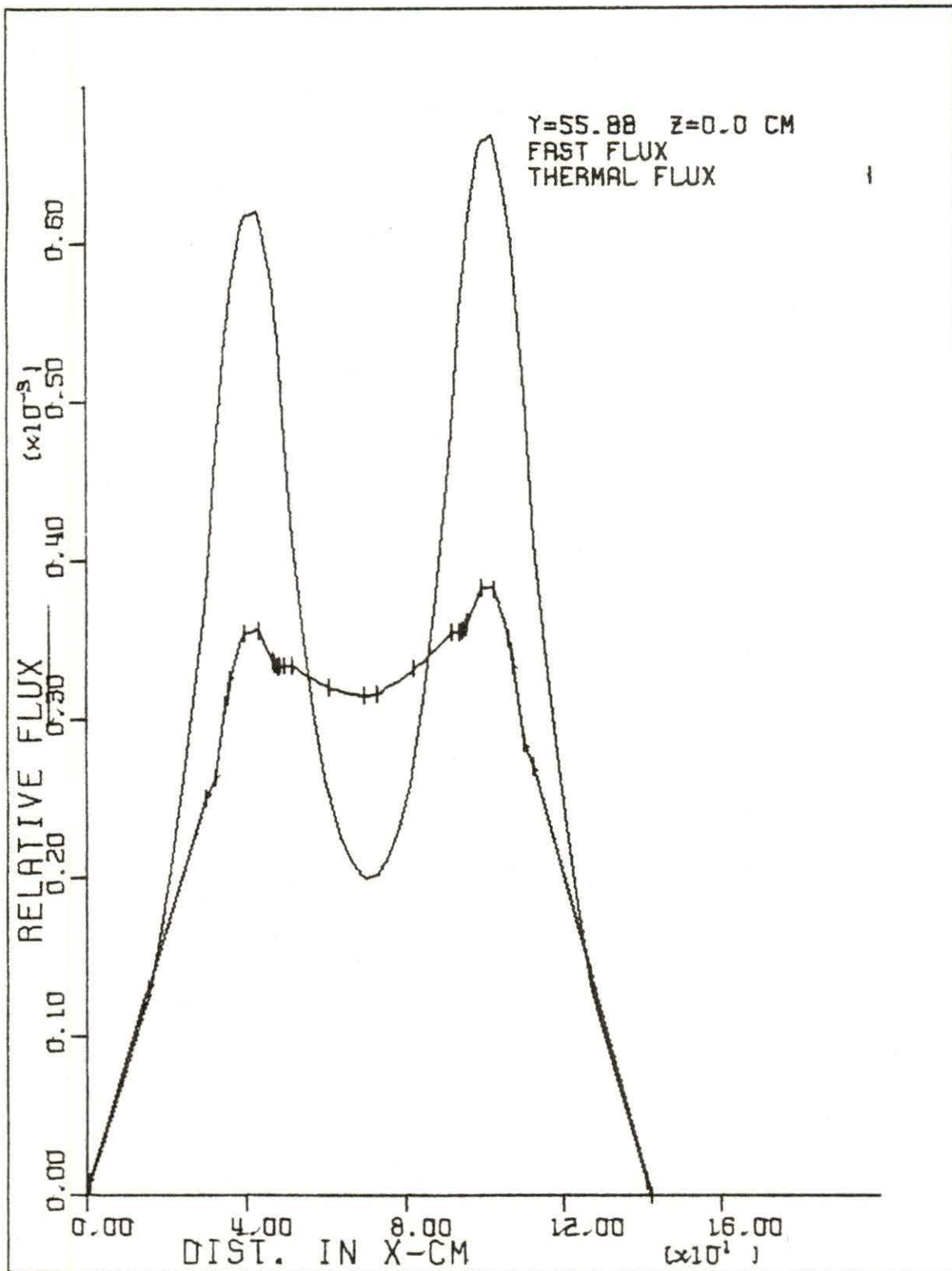


Figure 5.6. Fast and thermal flux distribution along the X-axis for the unperturbed core

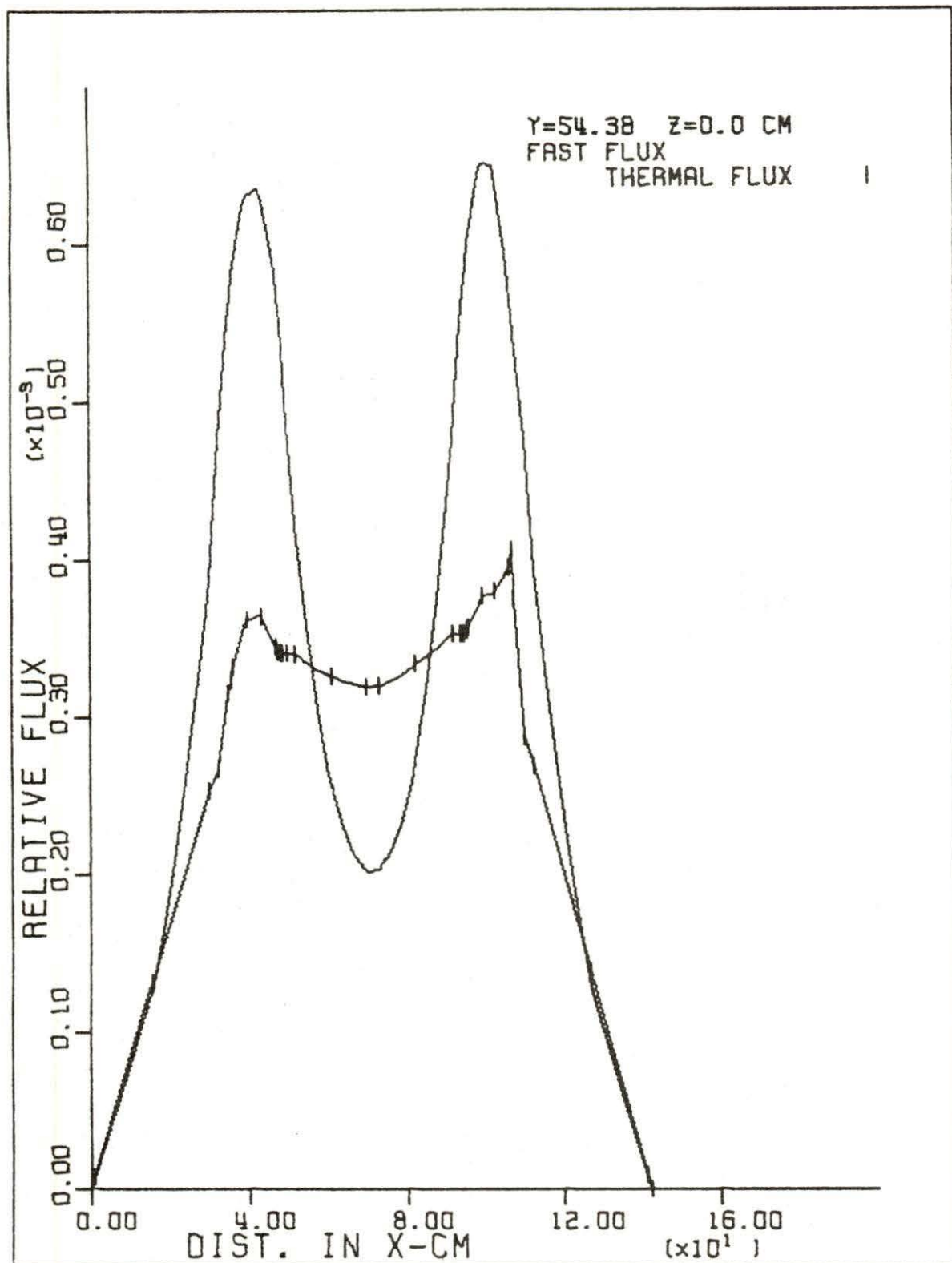


Figure 5.7. Fast and thermal flux distribution along the X-axis with the plate from assembly N-4 removed

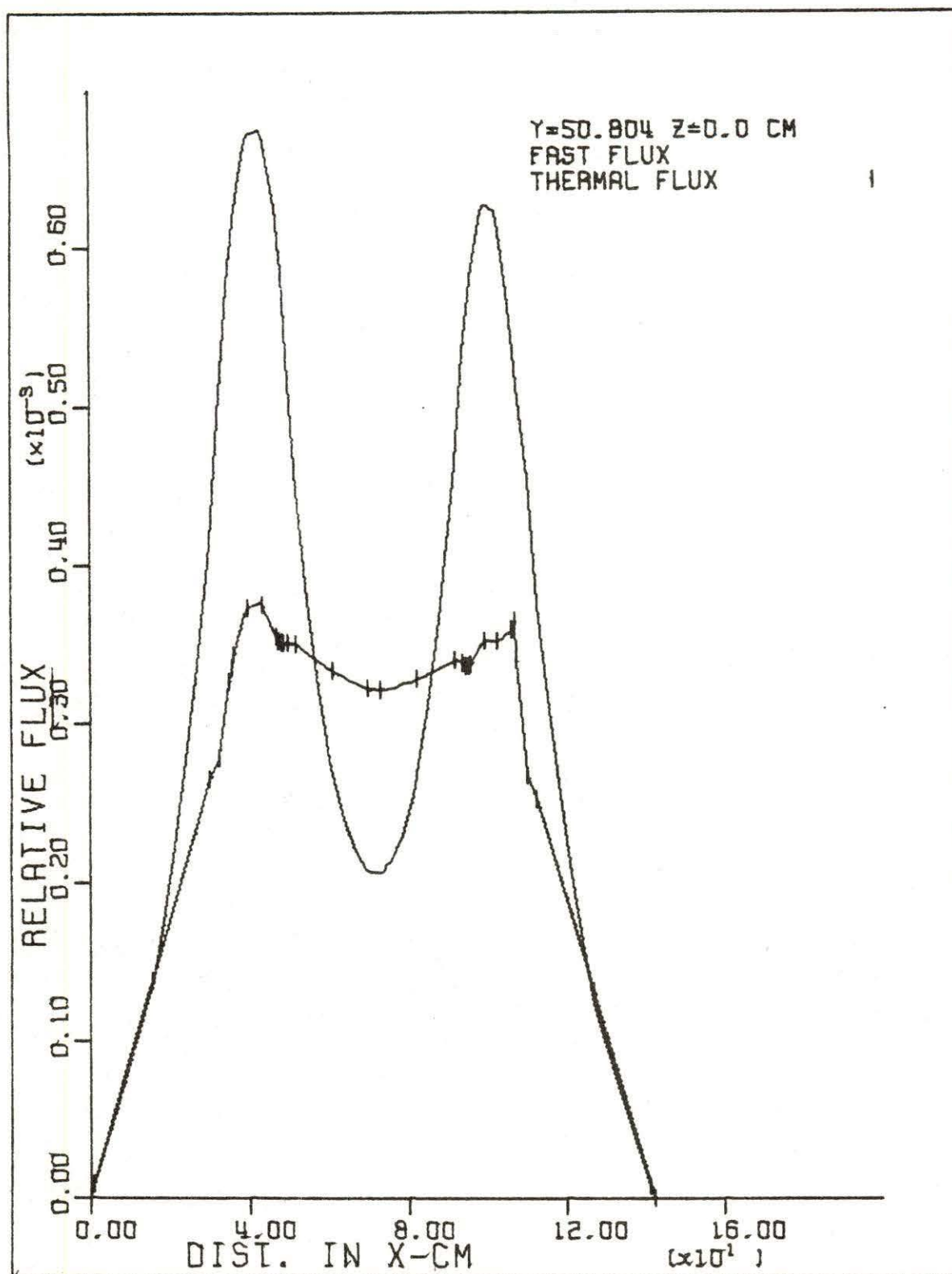


Figure 5.8. Fast and thermal flux distribution along the X-axis with the absorber region poisoned using $\Sigma'_p = 0.022108 \text{ cm}^{-1}$

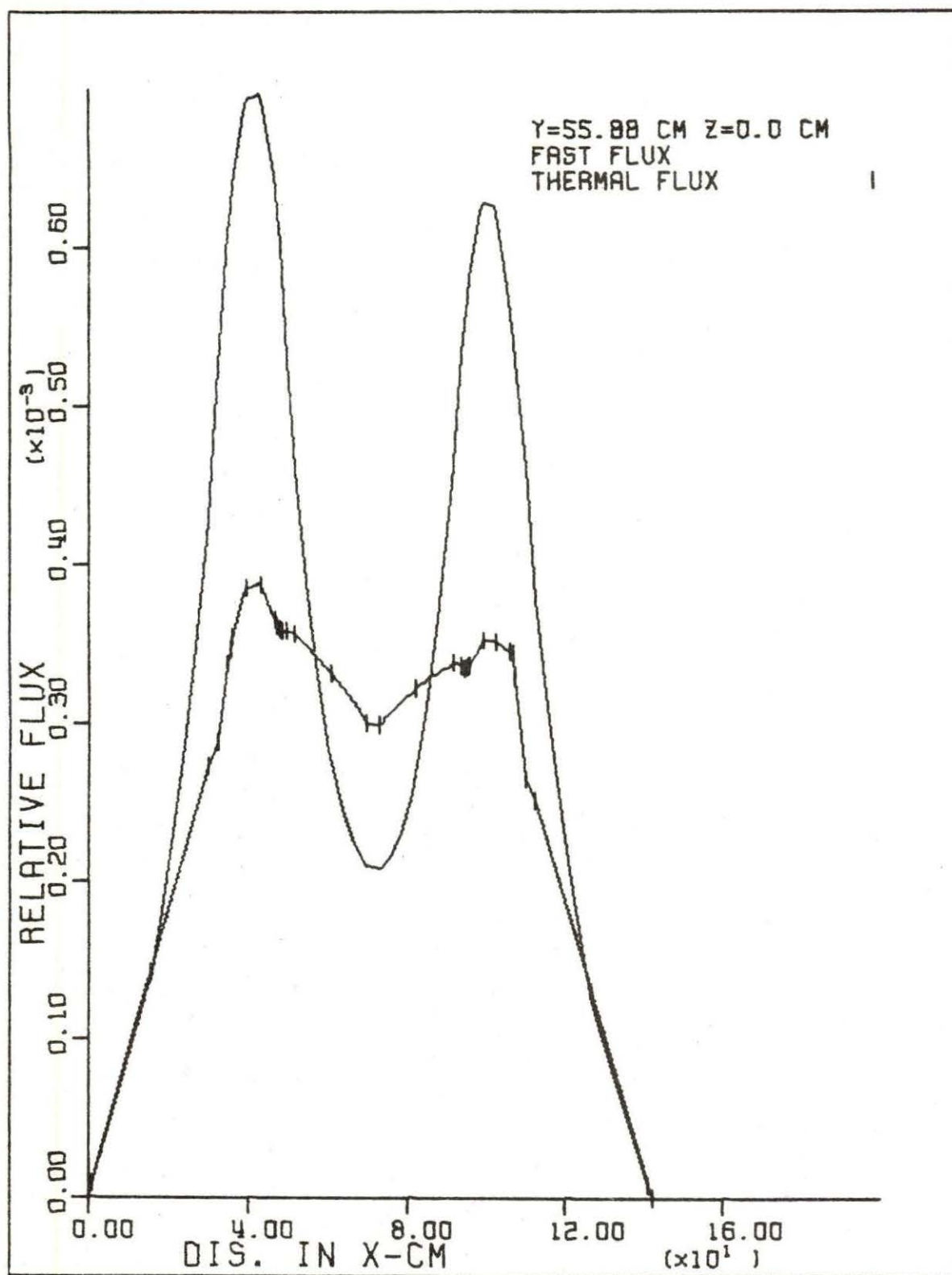


Figure 5.9. Fast and thermal flux distribution along the X-axis with the central detector region poisoned using $\Sigma_p = 0.036129 \text{ cm}^{-1}$

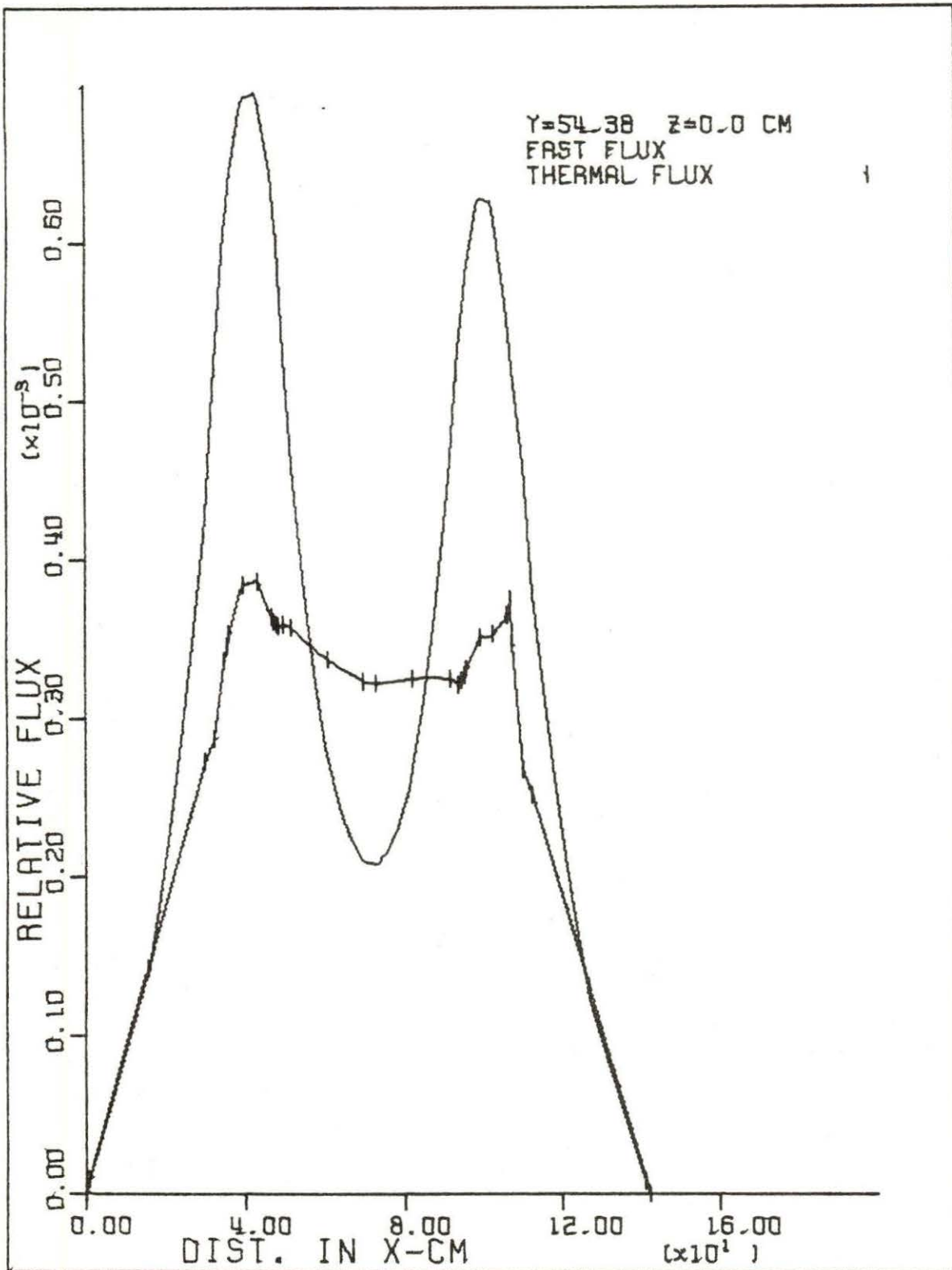


Figure 5.10. Fast and thermal flux distribution along the X-axis with the detector region at the side of the north core poisoned using $\Sigma_p = 0.0315 \text{ cm}^{-1}$

at the symmetry plane. Table 5.2 give a summarization of the results of these runs.

Table 5.2. Results of runs

$\Sigma_p \text{ cm}^{-1}$	$\Sigma'_p \text{ cm}^{-1}$	K_{eff}	Reactor condition
0	0	1.03436	Reference case
0	0	1.03153	Fuel plate removed
0.001917	0	1.00161	Both core uniformly poisoned
0.001917	0.022108	1.00063	Abs. region poisoned
0.036129	0	1.00002	Cent. stringer detector poisoned
0.0315	0	1.00002	North core side detector poisoned

B. The Adjoint Flux Calculation for Different Detector Positions

The theory developed in Chapter III was used to calculate the detector adjoint functions for the two group diffusion equations for the UTR-10 model by applying the equation

$$L^+ \phi^+ = \Sigma_d \quad (3.52)$$

where only the detector thermal macroscopic cross section was used in the calculation as follows

$$\Sigma_d = \begin{bmatrix} 0 \\ 1 \end{bmatrix} \quad (5.1)$$

The response of a neutron detector to a moving absorber was then found by using the equation

$$\Delta R = (\Sigma_d, \Delta\phi) = (\phi^\dagger, Q). \quad (5.2)$$

It is noted in Chapter III that a coupled set of neutron diffusion type equations must be solved, where the size of the system of equations is two times the number of energy groups used in the analysis.

Two detector positions in the UTR-10 reactor were used to calculate the adjoint functions using the computer code WHIRLAWAY. Figure 5.2 and Table 5.1 show the location of the detectors. The intervals between the absorber and the detector, which is located at the central stringer is 35.58 cm while the interval between the absorber and the detector at the side of the north core is 13.93 cm. Figure 5.11 shows the fast and thermal adjoint flux distributions along the X-axis with the detector at the central stringer. The sharp peak at the detector position is very noticeable. The thermal adjoint flux at the detector position is almost four times the fast adjoint flux. Also, Figure 5.12 shows a two-dimensional plot for the thermal adjoint function.

Figure 5.13 shows the fast and thermal adjoint flux distributions along the X-axis with the detector beside the north core. The sharp peak of the thermal adjoint flux at the detector position is almost three times the fast

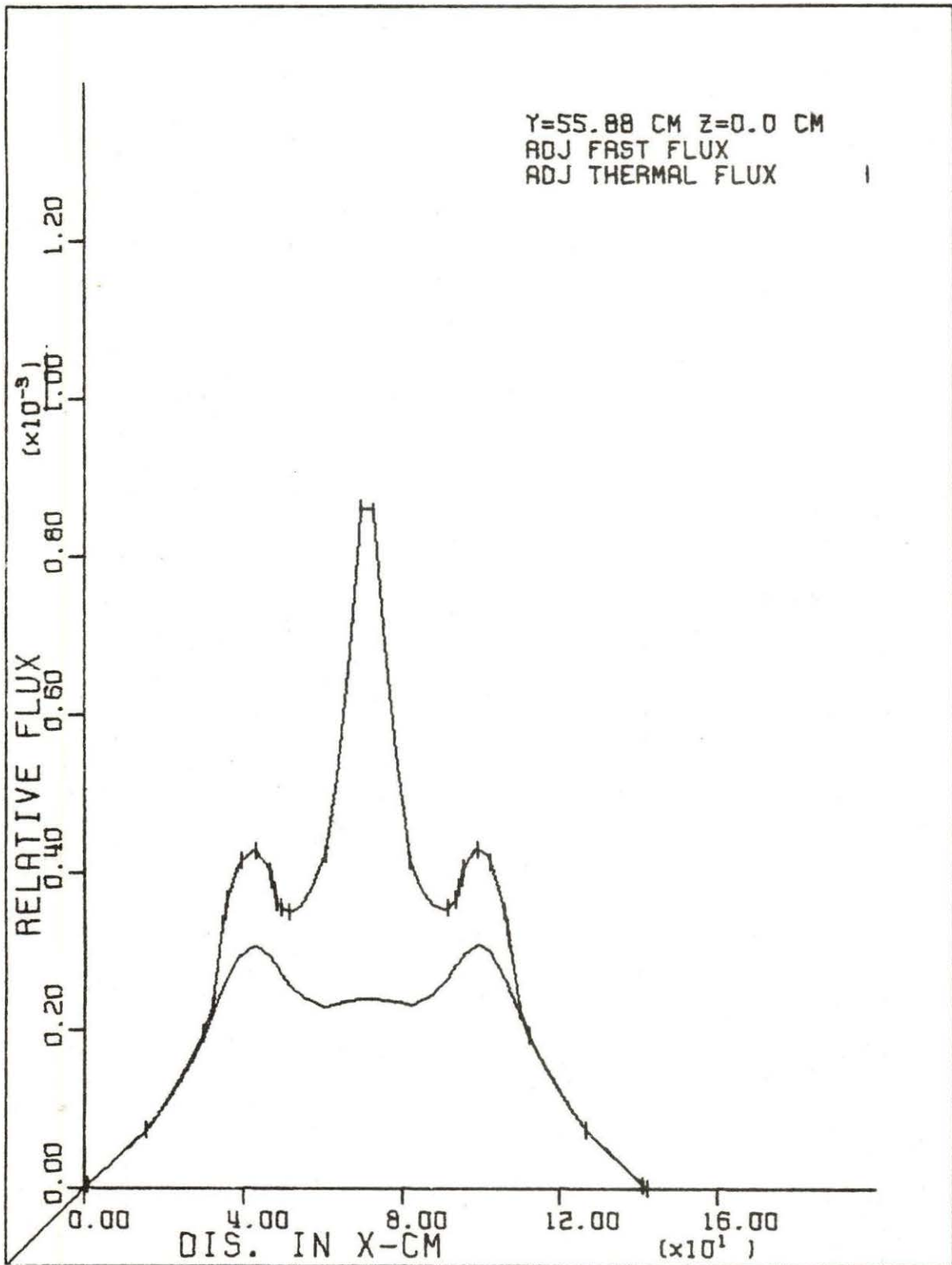


Figure 5.11. Fast and thermal adjoint flux distribution along the X-axis with the detector at the central stringer

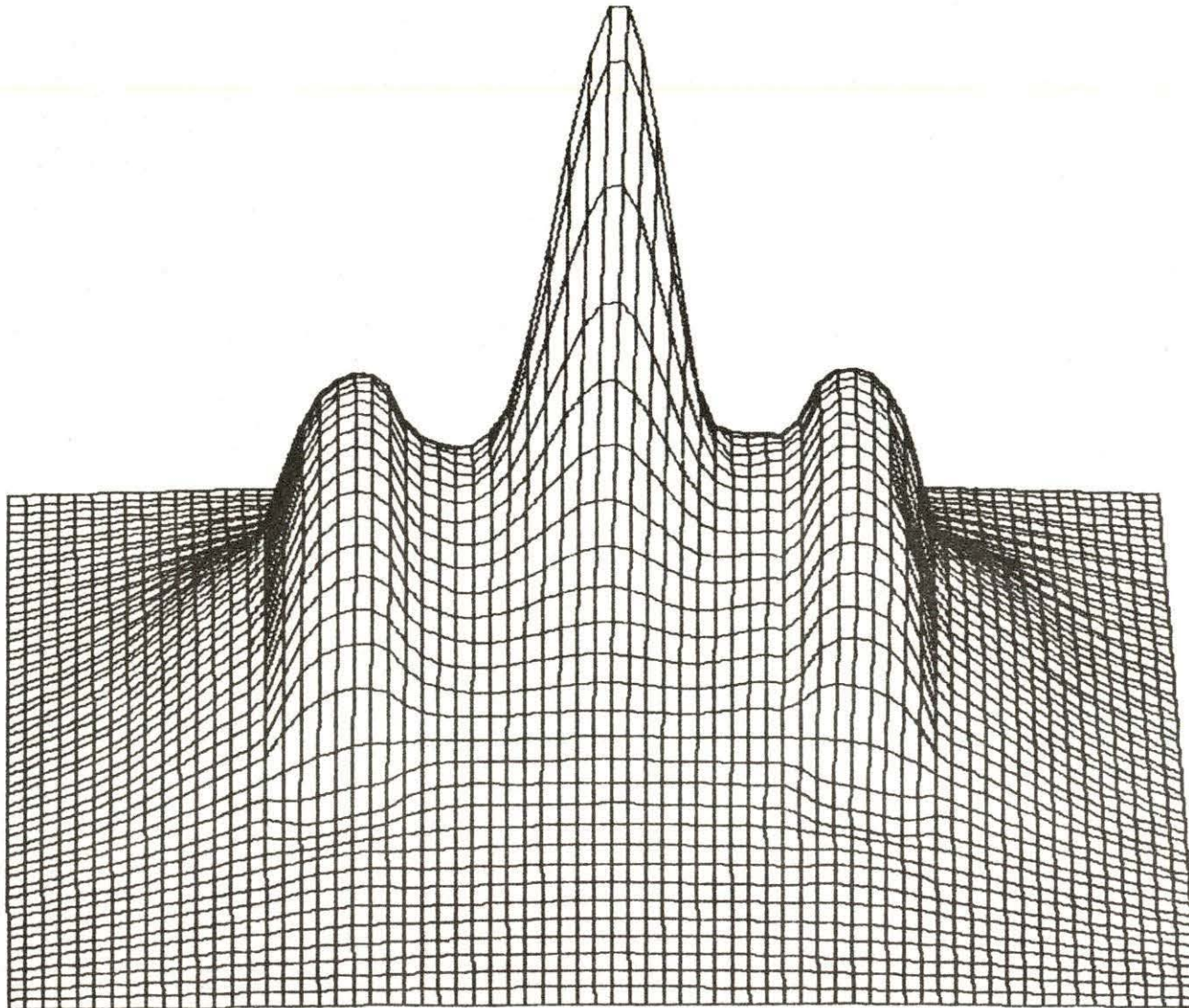


Figure 5.12. Two-dimensional plot for the thermal adjoint flux distribution at $Z = 0$ cm with the detector at the central stringer

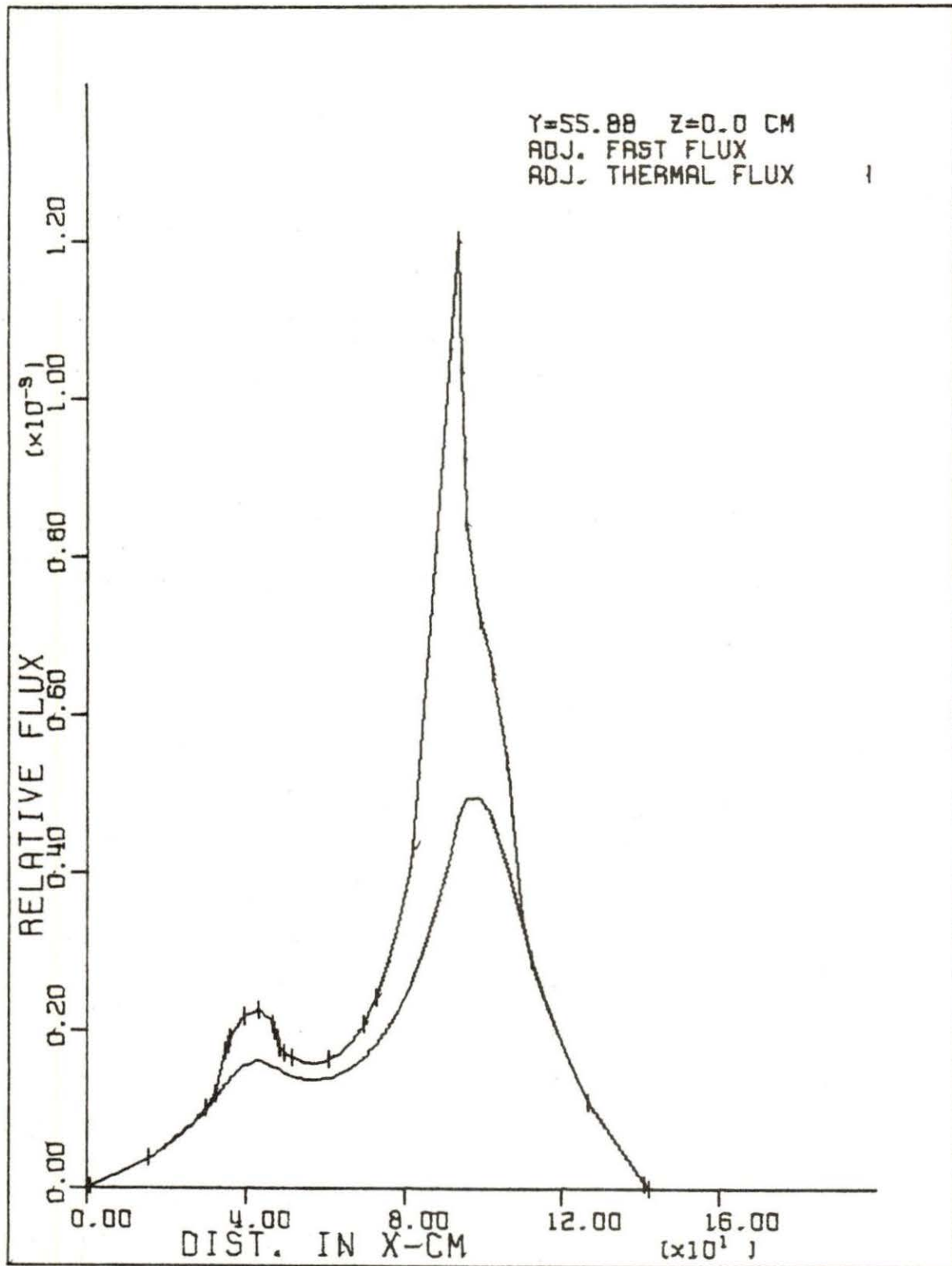


Figure 5.13. Fast and thermal adjoint flux distribution along the X-axis with the detector at the side of the north core

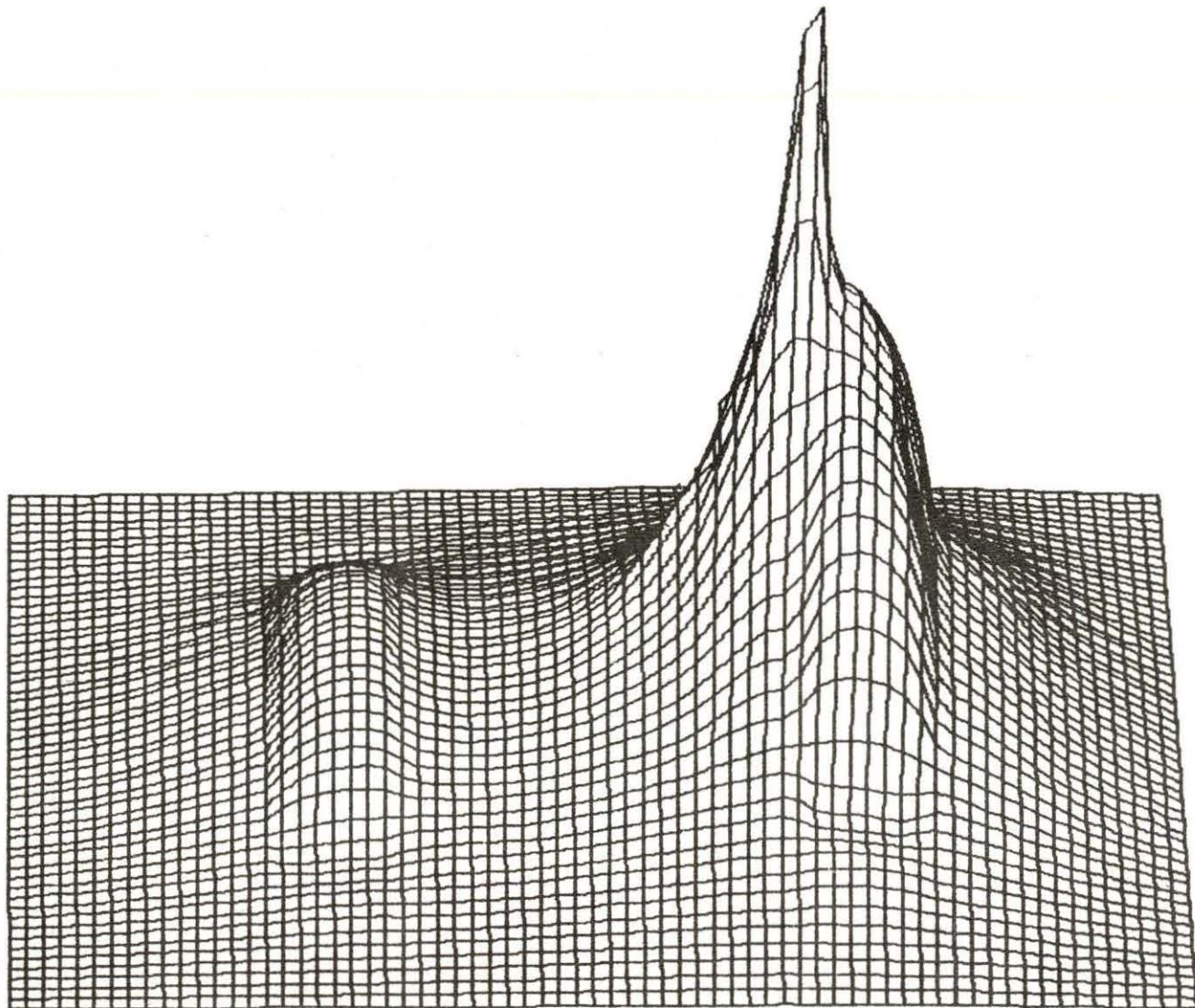


Figure 5.14. Two-dimensional plot for the thermal adjoint flux at $Z = 0$ cm with the detector at the side of the north core

adjoint flux. Figure 5.14 shows a two-dimensional plot for the thermal adjoint flux. In the next section there is more detail discussed about the significance of these adjoint function variations.

Table 5.3 compares the peaks of the fast and thermal adjoint values at both detector positions.

Table 5.3. The maximum fast and thermal adjoint flux values at different detector positions

Detector position	Fast adjoint relative flux	Thermal adjoint relative flux
At the central stringer	2.394×10^{-4}	8.606×10^{-4}
At the side of the north core	4.205×10^{-4}	1.203×10^{-3}

From Table 5.3 the significance of the detector position with respect to its distance from the core and the noise source can be seen.

C. Detector Response Function

The purpose of this work is to describe the calculation of the detector response to a moving absorber. Basically, the absorber vibration can be described by

$$\Delta \Sigma_{a_2} = \gamma [\delta(x-x_p + \epsilon) - \delta(x-x_p)] \quad (5.3)$$

where

γ = the absorber strength

x_p = the absorber location

ϵ = the displacement of the absorber

δ = delta function

Insertion of Equation 5.3 into Equation 5.2 yields

$$\Delta \phi_2 = \gamma \int_V \int_{-\infty}^{\infty} [\Delta(x-x_p + \epsilon(t)) - \Delta(x-x_p)] \phi_2 \phi_2^\dagger dx \exp(i\omega t) dt. \quad (5.4)$$

Carrying out the space integration for Equation (5.4)

yields

$$\begin{aligned} \Delta \phi_2 = \Delta \int_{-\infty}^{\infty} [\phi_2(x_p - \epsilon(t)) \phi_2^\dagger(x_p + \epsilon(t), x_0, \omega) \\ - \phi_2(x_p) \phi_2^\dagger(x_p, x_0, \omega)] e^{i\omega t} dt. \end{aligned} \quad (5.5)$$

Expanding Equation (5.5) in a Taylor's series of $\epsilon(t)$ yields

$$\begin{aligned} \Delta \phi_2(x_0, \omega) = \gamma [\phi_2(x_p) \left. \frac{\partial \phi_2^\dagger(x, x_0, \omega)}{\partial x} \right|_{x=x_p} \\ + \phi_2^\dagger \left. \frac{\partial \phi_2(x_p)}{\partial x} \right|_{x=x_p}] \epsilon(\omega). \end{aligned} \quad (5.6)$$

Equation (5.6) describes the effect of the moving absorber (noise source) on the thermal flux characteristic which represents the detector response to this perturbation. Table 5.4 shows the calculated parameters for Equation (5.6). Using the values determined for Equation (5.6) from Table 5.4 to evaluate the equation for both detector

Table 5.4. The parameters of Equation 5.6 for both detector locations

Detector location	$\phi_2(x_p)$	$\frac{\partial \phi_2^\dagger(x, x_0, \omega)}{\partial x}$	ϕ_2^\dagger	$\frac{\partial \phi_2(x)}{\partial x}$
At the central stringer	3.443×10^{-4}	0.2970×10^{-4}	3.317×10^{-4}	0.1411×10^{-4}
At the side of the north core	3.438×10^{-4}	0.4865×10^{-4}	5.099×10^{-4}	0.1403×10^{-4}

positions, the following results are obtained:

For the detector at the central stringer

$$\Delta \phi_2 = 1.4906 \times 10^{-8} \gamma \epsilon \quad (5.7)$$

and for the detector beside the north core

$$\Delta \phi_2 = 2.3880 \times 10^{-8} \gamma \epsilon . \quad (5.8)$$

From Equations (5.7) and (5.8), the significance of the detector position in the reactor can be seen. It is clear that the response of the detector beside the north core is greater than the response of the detector at the central stringer location by approximately 62%. This seems physically reasonable since it is closer to the core and the perturbation source. This analysis provides a working model for a proposed experimental investigation of

the detector response to a moving absorber located in the fuel region of the reactor. The calculated detector responses of Equations (5.7) and (5.8) which provide an indication of the detector response variation across the core, are useful for the planning of this experiment.

A preliminary design and safety analysis of a vibrator to be used in the reactor is presented in Appendix B. Also, computer programs for generating plots of neutron flux and adjoint function data are presented in Appendix A. Required JCL cards for use of the WHIRLAWAY code are presented in Appendix C.

VI. CONCLUSIONS

Based on the investigation carried out in this thesis, the following conclusions can be drawn:

1. From the results of the K_{eff} calculations, it has been found to be feasible to operate a vibrator assembly in the fuel region of the reactor. The reactor has been shown to be critical with one fuel plate removed from assembly N-4 and still have sufficient reactivity to be critical with neutron detectors and absorbers in place. The calculations that were performed are the most detailed that have ever been carried out for the UTR-10.

2. The detector adjoint calculations provide information on the response of a neutron detector in the central stringer location and beside the north core in the internal reflector. The response of detectors at either location appears to be suitable for measurement purposes. The detector nearest the north core will have a response about 62% greater than the central detector.

3. A preliminary design of a vibrator assembly for use in a fuel region has been developed. Based on this design it should be possible to prepare detailed engineering drawings and carry out construction of the system (Appendix B).

4. A method for handling large amounts of calculated flux and adjoint function data on tape has been documented and demonstrated with one and two-dimensional flux plots.

VII. SUGGESTIONS FOR FUTURE WORK

Some suggested extensions to this work include:

1. Performing experimental measurements for the vibrator and detector positions studied in this thesis. This would include carrying out a detailed design of the vibrator system that is described in a preliminary way in this work.
2. A two-dimensional calculation of the detector adjoint function could be calculated and compared with the three-dimensional model used in this research. A two-dimensional calculation would require less computer time and if adequate agreement is obtained between the two models, saving of funds could result.
3. A comparison of the real and imaginary parts of the adjoint function should be carried out using multidimensional models.
4. Additional calculations could be carried out for other locations in the reactor.

VIII. BIBLIOGRAPHY

1. G. T. Analytis, A three-dimensional theoretical investigation of the local and global component of neutron noise in bare homogeneous water moderator reactors and applications, *Annals of Nucl. Energy* 7, 351 (1980).
2. R. F. Barry, LEOPARD--A spectrum dependent non-spatial depletion code for the IBM-7094, WCAP-3269-26 (1963).
- ③. H. Van Dam, Neutron noise in boiling water reactors, *Atomkernergie* 27, No. 1, 8 (1976).
4. H. Van Dam, On the adjoint space in reactor noise theory, *Annals of Nucl. Energy* 4, 185 (1977).
- ⑤. J. J. Duterstadt and L. J. Hamilton, Nuclear reactor analysis (Wiley & Sons, Inc., New York, 1976).
6. T. B. Fowler and M. Tobias, WHIRLAWAY--A three-dimensional, two-group neutron diffusion code for IBM 7090 Computer, ORNL-3150 (1961).
7. E. Greenspan, On the adjoint space in reactor theory, *Annals of Nucl. Energy* 3, 323 (1976).
8. E. Greenspan, Some applications of the adjoint function in reactor theory, *Annals of Nucl. Energy* 3, 147 (1976).
9. F. B. Hildebrand, Methods of applied mathematics, 2nd ed. (Prentice-Hall Inc., New York, 1965).
10. L. R. Huang, Use of adjoint space models for predicting the response of a neutron detector to core parametric fluctuations, Ph.D. thesis, Iowa State University, 1979 (unpublished).
11. G. Kosaly, Remarks on a few problems in the theory of power reactor noise, *Nucl. Energy* 14, No. 3, 67 (1973).
12. G. Kosaly and L. Mesko, Investigation of the local component of power reactor noise via diffusion theory, Report of the Central Research Institute for Physics KFKI-75-27 (1975).

13. I. Pázsit, Two-group theory of noise in reflected reactors with application to vibrating absorbers, *Annals of Nucl. Energy* 5, 185 (1978).
14. I. Pázsit and G. T. Analytis, Theoretical investigation of the neutron noise diagnostics of two-dimensional control rod vibrations in a PWR, *Annals of Nucl. Energy* 7, 17 (1980).
15. M. Tobias, the EQUIPOISE METHOD--A simple procedure for few-group diffusion calculation in two and three-dimensions, *Nucl. Sci. Engr.* 12, 513 (1962).

IX. ACKNOWLEDGMENTS

The author wishes to express his sincere appreciation to his major professor, Dr. R. A. Danofsky for his valuable suggestions and discussions, and for his encouragement throughout the work. The author also wishes to express his appreciation to Dr. R. A. Hendrickson for his help by offering the UTR-10 data which is needed for this work. The author also wishes to acknowledge Mr. Abdul Mohsen Metwally for his encouragement, and for his helpful discussions throughout the courses. Acknowledgment should be expressed to the Government of Iraqi Republic for offering him the scholarship. The author also wishes to express his special appreciation to his wife, Eyda Salih, for her encouragement and her support through the years of study. Finally, the author wishes to express his sincere gratitude to his family for their encouragement and support through the years of study.

X. APPENDIX A: COMPUTER PROGRAMS

FOR PLOTTING

A. The One-Dimensional Plot
Computer Program

A one-dimensional computer program has been written to plot the calculated fluxes and adjoint fluxes. The user should provide the input data. The user also could change the X and Y labeling as desired. Also, the graph labeling could be changed. The listing of the program follows:

```

DIMENSION X(35), PH1(35), PH2(35), XL(5), YL(5)
X(1) = 0.0
PH1(1) = 0.0
PH2(1) = 0.0
READ(5,1)XL, YL
READ(5,2)(X(I), I = 2,35)
READ(5,3)(PH1(I), I = 2,35)
READ(5,4)(PH2(I), I = 2,35)
1  FORMAT(3X,5A4,1X,5A4)
2  FORMAT(8(E10.3))
3  FORMAT(8(E10.37))
4  FORMAT(8(E10.37))

CALL GRAPH(35,X,PH1,0,2,5.0,7.0,0.0,0.0,0.0,0.0,XL,YL,
*'Y=55.88 Z=0.0 CM;', 'FAST FLUX;')
CALL GRAPHs(35,X,PH2,13,101,'THERMAL FLUX;')
STOP
END

```

This program will provide plotting of two graphs for the fast and thermal flux.

B. Using Tapes in Running WHIRLAWAY
Code and the Two-Dimensional
Plot Computer Program

A two-dimensional plotting computer program has been written to plot the calculated fluxes by using data from the tapes. Two magnetic tapes have been used to store the WHIRLAWAY output. Tape number 11 contains four files as described in Table A.1 and tape number 12 contains three files as described in Table A.2.

Table A.1. Tape #11 (DAH1) files description

File #	DSN	Description
1	ADJCD	The 3rd plate from outside N-4 removed and both cores have been poisoned by $\Sigma_p = 0.001917$ and the detector region at the center of the reactor has been poisoned by $\Sigma_p = 0.036129$, also the absorber region poisoned by $\Sigma_p = 0.022108$, $K_{eff} = 1.00002$.
2	NCHNG	No change, no poison, $K_{eff} = 1.03397$.
3	ADJSR	Adjoint calculation for the detector located at the side of the north core, $K_{eff} = 1.00001$.
4	ADJCR	Adjoint calculation for the detector located at the center of the reactor, $K_{eff} = 1.00001$.

Table A.2. Tape #12 (T2515) files description

File #	DSN	Description
1	File 2	3rd plate from N-4 removed, both cores poisoned by $\Sigma_p = 0.001917$, $K_{eff} = 1.00161$
2	ABSRE	3rd plate from outside N-4 removed, both cores poisoned by $\Sigma_p = 0.001917$ and absor. region poisoned by $\Sigma_p = 0.022108$, also the detector region beside the north core from inside poisoned by $\Sigma_p = 0.0315$, $K_{eff} = 1.00002$
3	NCHNG	No change, no poison

For creating many files in each tape, the file number and the data set name (DSN) should be changed in the job control cards belonging to the unit in each case. For example, in the first run the output has been created from zero initial fluxes, say file number 1 in tape 11 with the DSN = ADJCD. For the next run, the initial fluxes are read from tape number 11 and the output fluxes stored on tape number 12. This could be done by putting one as a file number 1 and DSN = File 2 on unit 12. The JCL cards to be used with the WHIRLAWAY code for this example are described as follows:

```
//FT11F001 DD DISP = (NEW,KEEP),
// UNIT = (TAPE,,DEFER), VOL=SER=DAH1,LABEL(1,SL),
//          DSN=ADJCD,
// DCB = (RECFM=VBS,LRECL=1596,BLKSIZE=1600)
//FT12F001 DD DISP = (NEW,KEEP),UNIT=(TAPE,,DEFER),
//          VOL=SER=T2515,LABEL=(1,SL),DSN=FILE2,
//          DSB=(RECFM=VBS,LRECL=1596,BLKSIZE=1600)
```

For the next run, creating the second file on unit 11 could be done as follows and so on.

```
//FT11F001 DD DISP=(NEW,KEEP),
// UNIT=(TAPE,,DEFER),VOL=SER=DAH1,LABEL(2,SL),DSN=NCHNG,
// DCB=(RECFM=VBS,LRECL=1596,BLKSIZE=1600)
//FT12F001 DD DISP=(NEW,KEEP),UNIT=(TAPE,,DEFER),
// VOL=SER=T2515,LABEL=(1,SL),DSN=FILE2,
// DSB=(RECFM=VBS,LRECL=1596,BLKSIZE=1600)
```

Since both regular and adjoint fluxes are calculated when the adjoint function is calculated two files from the regular fluxes must be used as an input of initial fluxes to the code. The required JCL cards are as follows:

```
//FT11F001 DD DISP=(NEW,KEEP),UNIT=(TAPE,,DEFER),
// VOL=SER=DAH1,LAEBL=(4,SL),DSN=ADJCR,
// DCB=(RECFM=FBS,LRECL=1596,BLKSIZE=1600)
//FT12f001 DD DISP=(NEW,KEEP),UNIT=(TAPE,,DEFER),
// VOL=SER=T2515,LABEL=(2,SL),DSN=ABSRE,
// DCB=RECFM=VBS,LRECL=1596,BLKSIZE=1600)
// DD DISP=(NEW,KEEP),UNIT=(TAPE,,DEFER),
// VOL=SER=T2515,LABEL=(3,SL),DSN=NCHNG
```

This would create file number 4 with the name ACJCR on tape number 11 by using the data stored on files 2 and 3 from tape number 12.

Listing of the two-dimensional plotting computer program is as follows:

```
C USE THIRD2 TO CREAT 3 DIMENSIONAL PLOTS OF A
C HYPERBOLIC PARABOLOID (SADDLE SURFACE).
REAL*4 DATE(7),PARM(11),A(70,27)
REAL*4 P(11340)
REAL*4 PP(35,27)
REAL*4 XL(70),YL(54),WK(213),X(35),Y(27)
CALL LABEL (DATE, PARM, NPARM)
ANGA = -90.*3.141593 / 180.0
ANGB = 45.0*3.141593 / 180.0
```



```

HV = 7.0
KODE = 3
READ(11)      (Skips fast regular flux)
READ(11)      (Skips thermal regular flux)
READ(11)      (Skips fast adjoint flux)
READ(11)P     (Plot the thermal adjoint flux)
N=2
DO 1 I=1,35
DO 1 J=1,27
PP(I,J)=P(N)
1  N=N+12
   X(1) = 0.0
   Y(1) = 0.0
   READ(5,2)(X(I), I = 2,35)
2  FORMAT(8(F10.3))
   READ(5,2)(Y(I), I = 2,27)
   NX = 70
   XL(1) = 2.0
   DO 15 I = 2,NX
15  XL(I) = XL(I-1)+2.0
   NY = 54
   YL(1) = 2.0
   DO 20 J = 2,NY
20  YL(J) = YL(J-1)+2.0
   CALL IBCIEU(PP,35,X,35,Y,27,XL,NX,YL,NY,A,70,WK,IER)
   CALL THIRD2(A,NX,NY,KODE,ANGA,ANGB,HV,70)
   CALL ENDPLT
   STOP
   END

```

The above program will provide a two-dimensional plot for the thermal adjoint flux. To plot the regular thermal flux change the read statements to

```

READ(11)
READ(11)P

```

This program reads calculated fluxes from tape on unit 11. The required JCL cards to be used with the program are as follows:

```
//STEP1 EXEC FORTG,LIB='SYS1.PLOTLIB',REGION.GO=128K
//FORT.SYSIN DD *
        PROGRAM
//GO.SYSIN DD *
        X AND Y INTEVALS DATA
//GO.PLOTTAPE DD SYSOUT=(W,PLOTWTR)
//GO.FT11F001 DD DISP=(NEW,KEEP),UNIT=(TAPE,,DEFER),
//  VOL=SER=DAHL,LABEL=(4,SL),DSN=ADJCR,
//  DCB=(RECFM=VBS,LRECL=1596,BLKSIZE=1600)
//
```

XI. APPENDIX B

A. Description of Vibrator
Assembly

Experimental work for measuring the neutron detector response to a moving absorber has been suggested. Analytical calculations were carried out for the case of an absorber placed in the area shown in Figure B.1, where the absorber is estimated to have an equivalent worth of approximately 15¢. The dimensions of the absorber region are 2.235 cm x 3.576 cm. The proposed position for a neutron detector, in addition to other choices of detector positions, is also shown in Figure B.1.

The vibrator model and the apparatus to be used in the proposed experiment are shown in Figure B.2.

This device is intended to simulate a vibrating or moving core component and consists of a moving aluminum rod holding a cadmium absorber, magnetic coils for actuating the vibrating rod, and a linear variable differential transformer (LVDT) for sensing the motion of the absorber. The assembly is clamped to the top of the core tank to hold it in position, and is designed such that it can be positioned to move in either a North-South or East-West direction. The magnetic coils can be energized by a power supply and relay driven by a square wave to obtain periodic motion or

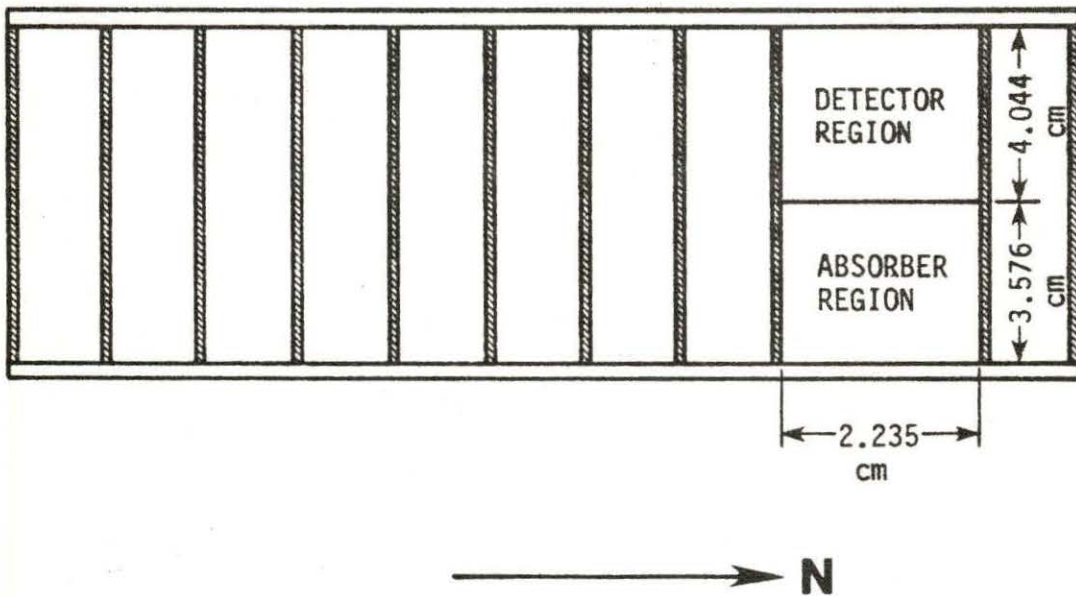


Figure B.1. Fuel assembly N-4 with the detector and the absorber regions shown

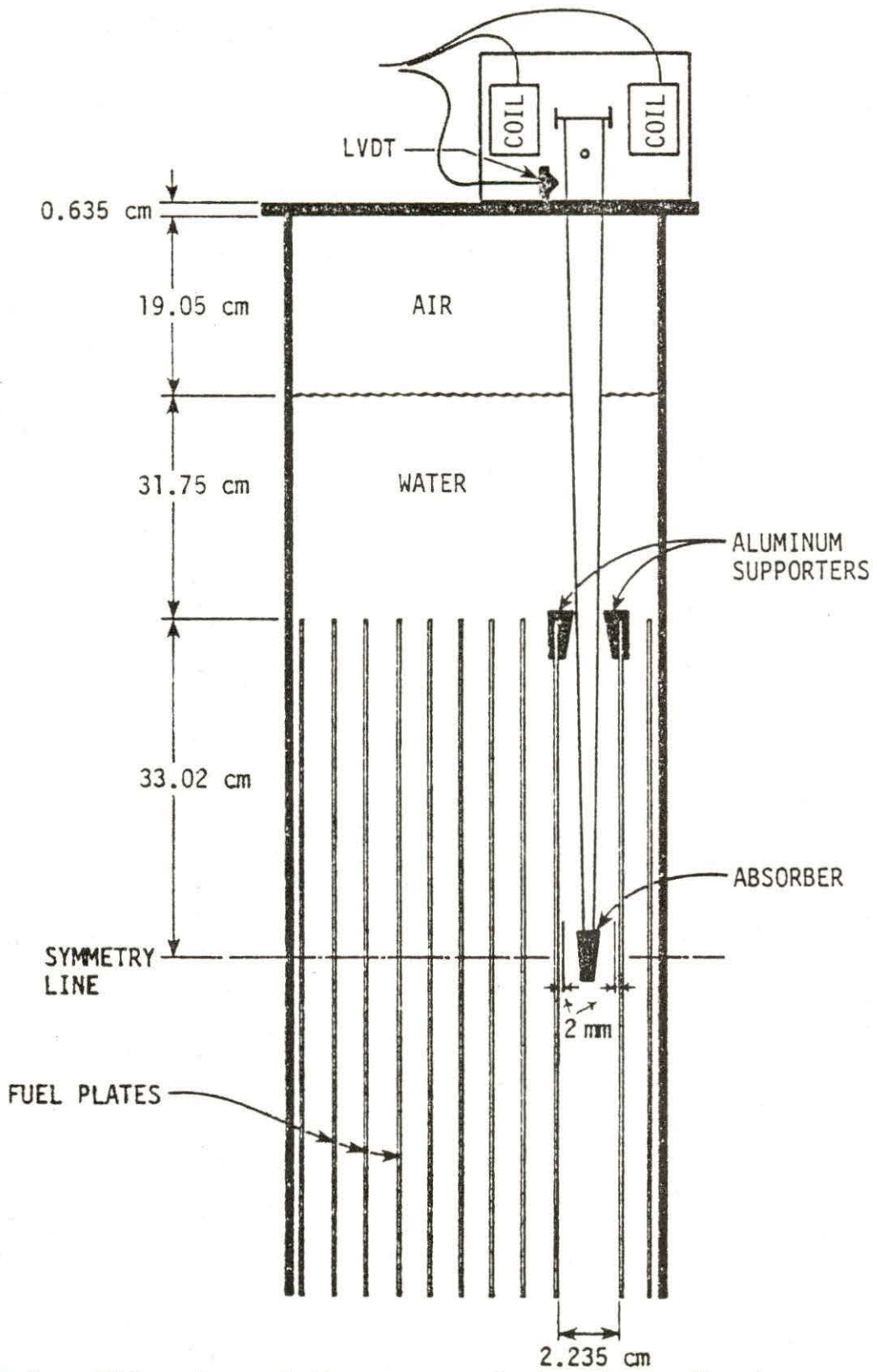


Figure B.2. Side view of the proposed absorber vibrator inside assembly N-4

by a pseudo random input to obtain wide band noise. Careful considerations should be given in the design to prevent any contact between the absorber and the fuel plates. A space of 2 mm has been left on both sides of the fuel plates in the absorber region. The distance that the absorber is going to travel is 1.835 cm. Since the top 1.5 inches of the fuel plate is aluminum (no fuel), there is no hazard involved in placing aluminum supporters to control the motion of the aluminum rod holding the absorber.

To increase the material stiffness it is suggested that the aluminum rod be machined with a taper. Since aluminum is the major material in the core, activation should not be a significant problem.

If for some reasons the absorber should drop out of the core, a significant hazard does not result since the worth is very small ($\leq 15\phi$). The absorber holder in the core, is going to displace an equivalent volume of water. The thermal macroscopic absorption cross section for the aluminum is 0.015 cm^{-1} while the thermal macroscopic absorption cross section for the water is 0.01878 cm^{-1} for a difference of 0.00378 cm^{-1} . Therefore, replacement of the aluminum by water actually increases the absorption cross section of the core. Since the volume of aluminum that is going to displace water is quite small, the effects on the flux shape is negligible.

It is concluded that the vibrator assembly can be safely placed and operated in the UTR-10 reactor.

B. Preliminary Safety Analysis
Report for the
Proposed Experiment

This analysis follows that required for experiments to be placed in the UTR-10 reactor.

1,2. Description and location of materials to be inserted in reactor:

The experimental vibrating absorber shown in Figure B.2 is to be inserted in fuel assembly N-4 shown in Figure B.1. As shown in Figure B.1, the third fuel plate from the north side of the element has been removed to provide room for the absorber. It is also possible that a neutron detector will be placed in this same region as shown.

3. Flux level and duration of experiment

$$\phi \leq 1.8 \times 10^{10} \text{ n/cm}^2 \cdot \text{s at 3 kw}$$

$$t \leq 2 \text{ hours}$$

It is estimated that the maximum power level used in the experiment will be 3 kw and the maximum duration of the experiment at any one time will not exceed 2 hours.

4. The materials to be inserted in the reactor consists of the following:

Cd sheet 2" x 1" x 0.02" (5.8 cm x 2.54 cm x 0.05 cm)

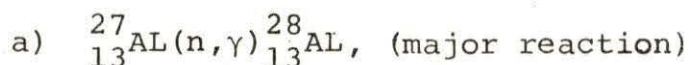
Al cone shaped rod: 35.47 cm (long)

1.5 cm (upper diameter)

0.2 cm (lower diameter)

Masking tape: to be wrapped around the absorber (Cd sheet) and the aluminum rod, to hold the absorber in place. The electrical coils and wires are placed above the water region in the core and are assumed to not be significantly activated.

5. Nuclear reactions:



$$\Sigma_a = 0.015 \text{ cm}^{-1}, T_{1/2} = 144 \text{ sec}$$

- b) $\text{Cd}(n,\gamma)$ (no significant activation from previous experience)

$$\Sigma_a = 114 \text{ cm}^{-1}, T_{1/2} = 23400 \text{ sec}$$

6. Calculation of activities: For aluminum

$$T_{1/2} = 144 \text{ sec}, \lambda = \frac{0.693}{T_{1/2}} = \frac{0.693}{144} = 0.00481 \text{ sec}^{-1}$$

$$N = \frac{V \rho Av.}{27} = \frac{14.55 \times 2.699 \times 6.022045 \times 10^{23}}{26.98} = 8.77 \times 10^{23}$$

$$\Sigma_a = N \sigma_a = 8.765 \times 10^{23} \times 0.241 \times 10^{-24} = 0.211 \text{ cm}^{-1}$$

The activity after shutdown is:

$$\text{Activity } (A_0) = \frac{\Sigma a \phi}{\lambda} = \frac{0.211 \times 1.8 \times 10^{10}}{0.0048125}$$

$$A_0 = 7.90 \times 10^{11} \text{ dis/sec} = 21.35 \text{ Ci}$$

The activity at 16 hours after shutdown is:

$$\begin{aligned} A &= A_0 e^{-\lambda t} \\ &= 21.35 e^{-0.0048125 \times 57600} \\ &= 2.135 \times 10^{-98} \text{ Ci} \end{aligned}$$

This could be neglected since it is a very small activity (≈ 0).

7. Potential hazards of experiment. The major potential hazard associated with the experiment would result from a loss of the cadmium absorber from the vibrator. To minimize the effect if this would happen, the worth of the cadmium will be at most 15¢ which would result in an asymptotic period of 56 seconds. This is well within the range of the operator and control system response time. It is also planned that the system will be tested extensively before insertion in the reactor to insure that the cadmium connection is secure.

Activation should not be a problem since aluminum has a short half life.

8. Storage and disposal of irradiated material: The assembly will be left in the reactor after shutdown for 16 hours before being taken to storage. If necessary, a temporary shield will be provided for storage.
9. Upon completion of the experiment, any activated components will be given to the University Environmental Health and Safety Group for permanent disposal.
10. Formal courses in nuclear physics, radioactivity, and radiation safety to be taken by the investigator:
 - a) Nuclear radiation measurement (NUC E 510)
 - b) Reactor Engineering Laboratory (NUC E 541)

XII. APPENDIX C: THE REQUIRED JCL FOR
 RUNNING WHIRLWAY CODE

The JCL needed to run the computer code WHIRLWAY and the plotting JCL cards can be described as follows:

To take a copy of the program from the tape to a disk the following JCL's are required for the first run only:

```
//S1 EXEC MOVE
//TAPE DD UNIT=(TAPE,,DEFER),VOL=SER=SALIH1,DISP=(OLD,
      PASS),
//  DCB=(RECFM=FB,LRECL=80,BLKSIZE=800),LABEL=(,NL)
//SYSIN DD *
      COPY PDS=S.15555.WHIRWAY,FORM=TAPE=(SALIH1,3),
      TO=DISK=SHORT1,
      FORMDD=TAPE
```

For running the code the following JCL's are needed:

```
//S2 EXEC PGM=WHIRWAY,TIME=(2,59),REGION=256K
//STEPLIB DD DSN=S.15555.WHIRWAY,DISP=SHR,UNIT=DISK,
      VOL=SER=SHORT1
//FTDGF001 DD SYSOUT=A
//FT08F001 DD UNIT=SCRATCH,SPACE=(TRK,(10,10)),DSNAME=&&A,
//DCB=(RECFM=VBS,LRECL=796,BLKSIZE=800),DISP=(NEW,DELETE)
//FT09001 DD SYSOUT=A,DCB=(RECFM=FBA,LRECL=133,BLKSIZE=133)
//FT11F001 DD DISP=(NEW,KEEP,UNIT=(TAPE,,DEFER),
//  VOL=SER=DAH1,LABEL=(4,SL),DSN=ADJCR,
//  DCB=(RECFM=VBS,LRECL=1596,BLKSIZE=1600)
//FT12F001 DD DISP=(NEW,KEEP),UNIT=(TAPE,,DEFER),
//  VOL=SER=T2515,LABEL=(2,SL),DSN=ABSRE,
//  DCB=(RECFM=VBS,LRECL=1596,BLKSIZE=1600)
//  DD DISP=(NEW,KEEP),UNIT=(TAPE,,DEFER),
//  VOL=SER=T2515,LABEL=(3,SL)DSN=NCHNG
//FT10F001 DD *
      (THE INPUT DATA CARDS)
```

The JCL's needed for plotting are:

```
//GO.FT14F001 DD DSNAME=&SM,UNIT=SCRATCH,DISP=(NEW,PASS),
//  SPACE=(800,(120,15)),DCB=(RECFM=VBS,LRECL=796,
      BLKSIZE=800)
//SMPLTR EXEC PLOT,PLOTTER=INCRMNTL,FORM=W
/*
```